



Two test-cases for synergistic detections in the Martian atmosphere: Carbon monoxide and methane



S. Robert ^{a,*}, C. Camy-Peyret ^b, F. Daerden ^a, M. De Maizière ^a, E. De Wachter ^a, L. Neary ^a, S. Vandenbussche ^a, A.C. Vandaele ^a

^a BIRA-IASB, Royal Belgian Institute for Space Aeronomy, 3 Ave Circulaire, B-1180 Brussels, Belgium

^b IPSL (UPMC&UVSQ), Paris, France

ARTICLE INFO

Article history:

Received 3 February 2016

Received in revised form

26 October 2016

Accepted 8 November 2016

Available online 20 November 2016

Keywords:

Mars

Martian atmosphere

Infrared

Future mission preparation

ExoMars

Trace Gas Orbiter

CH₄

CO

ABSTRACT

In the frame of the scientific preparation of ExoMars Trace Gas Orbiter (EMTGO), synergistic retrievals were performed on synthetic spectra of two different remote sensing instruments of the Martian atmosphere. To benefit from their diversity, we have simulated spectra of a Fourier transform spectrometer (FTS), working in the middle to far infrared and of a grating spectrometer (GA) working in the middle infrared. As control runs, non-synergistic retrievals were performed as well. Two molecules of interest in the Martian atmosphere were chosen to test this method: carbon monoxide and methane. Scenarios were selected and two different vibrational bands for each molecule were used to retrieve molecular volume mixing ratios. Synergistic retrievals for CO are useful both in solar occultation and in nadir, while for CH₄, the concentration of which is expected to be very low, the results for FTS and GA in synergy are not as conclusive due to the weak signal in the ν₄ vibrational band (covered by FTS) compared to the stronger ν₃ band (covered by GA). Our results represent a first step to an optimized use of infrared spectra to be recorded in Martian orbit by two instruments of EMTGO.

© 2016 The Authors. Published by Elsevier Ltd. This is an open access article under the CC BY-NC-ND license (<http://creativecommons.org/licenses/by-nc-nd/4.0/>).

1. Introduction

Synergies between different types of infrared instruments have been investigated in this study in view of improving the investigation of the Martian atmosphere. Synergistic studies have been performed on test-cases when studying Earth's atmosphere [1,2]. These synergies enable to increase the scientific return of the missions. In the planetary community, this approach has been limited to a theoretical point of view [3]. The objective of our study is to highlight the potential improvements resulting from the capabilities of combined multi-instrument platforms. This study should help in defining payloads for future missions by considering the complementarity between different techniques and spectral regions (spectral synergy). It could also be the first step in a better definition of the observation scenarios. This, in fact, was the starting point of our study, i.e. improve the synergistic operations of two instruments which will be part of the ExoMars Trace Gas Orbiter (EMTGO) mission [4]. The Royal Belgian Institute for Space Aeronomy (BIRA-IASB) is indeed heavily involved in the design, manufacturing, operations and science of the spectrometer suite

Nadir and Occultation for Mars Discovery (NOMAD) on board EMTGO [5,6]. On the same spacecraft, another instrument provided by Russia, the Atmospheric Chemistry Suite (ACS) [7], has been accommodated, which offers the possibility of combined observations with NOMAD.

Two species, carbon monoxide and methane, have been considered, both being important for a better understanding of the atmospheric composition and of the different processes taking place at the interface between the surface and the atmosphere. Measurements of CO and CH₄ on Mars have been performed both by Earth-based spectrometers and by several space instruments orbiting Mars [8–21], i.e. the Planetary Fourier transform Spectrometer (PFS) on Mars Express [22] or the Compact Reconnaissance Imaging Spectrometer for Mars (CRISM) on Mars Reconnaissance Orbiter (MRO) [4,23]. Several future missions to Mars are ongoing or under preparation but not all of them contain instruments able to perform a spectroscopic inventory of the neutral atmosphere. Indeed the only mission that will embark such instruments is EMTGO, successfully inserted in orbit in October 2016.

The remote sensing of CO and CH₄ from space can be performed in different spectral domains, in particular in the thermal infrared (TIR i.e. 5–25 μm) and the mid-wave infrared (MIR i.e. 2–5 μm), and under different geometries (nadir or limb observation viewing).

* Corresponding author.

E-mail address: severine.robert@aeronomie.be (S. Robert).

Because each of these spectral regions and geometries has its advantages and disadvantages, the possibilities to combine several types of measurements in a synergistic way have been studied in order to better exploit the data available in the near future, in particular to assess the near-surface processes. The challenge is to better capture CO and CH₄ information as close as possible to the associated sources, for improving the understanding, quantification or monitoring of sources and sinks of molecular species in the Martian atmosphere.

CO is a non-condensable gas and its seasonal behaviour can be used to constrain the expected behaviour of other non-condensable gases. The CO seasonal-spatial distribution on Mars is in fact very similar to that of argon, the reference non-condensable gas on Mars [24,25]. Strong deviations of the (to be measured) methane distribution from the one of relatively passive tracers would represent additional indications for the presence of active local sources of CH₄. Indeed, the Martian atmosphere contains several non-condensable gases, such as Ar, N₂ and CO. All these gases are expected to show similar behaviour: seasonal accumulation in polar regions during winter; dilution and transport to low latitudes in late winter and spring; depletion below average value during summer at some latitudes; hydrostatic instability and vertical mixing.

A synthetic dataset of spectra was created for various scenarios. Different parameters were chosen to get a statistical sample of spectra representative of the expected measurements. Then retrievals were performed considering non-synergistic and synergistic observations and analyses. The results of the fitting procedure and the benefits of the synergies are discussed.

2. Database of spectra

The purpose of this study is to investigate the improvement induced by considering the complementarity of different instruments and the analysis is based on simulated spectra. However, in order to investigate realistic payload configurations and because the ExoMars Trace Gas Orbiter (EMTGO) mission is the latest mission toward Mars embarking spectroscopic instruments, we have considered two instruments whose characteristics are very close to those of the real instruments on board the EMTGO mission, i.e. NOMAD and ACS. In this section, we will describe the radiative transfer modular program used to simulate the spectra and to retrieve the trace species abundances. The two instruments of interest will be described and selected scenarios will be presented.

2.1. Instrument specifications

The scientific objectives of the EMTGO mission are well defined [26,27] but the exact performances in orbit of all the instruments relevant for this activity are not yet known in detail. Two instruments will probe the infrared range and will be able to search for trace species in the Martian atmosphere, i.e. NOMAD and ACS [4]. We used them as a baseline to define the two representative instruments considered in this study. The specifications retained here are based mainly on the initial proposals of both experiments, with additional information from more recent and updated instrument status [5,6,28–31]. Nevertheless, some characteristics might not be the final ones and this paper should not be considered as a reference document comparing the exact characteristics of the two instruments which may have changed during the design and manufacturing process and may suffer from launch and cruise.

NOMAD has been selected by ESA and NASA to be part of the payload of the EMTGO mission [32]. This instrument suite will

conduct a spectroscopic survey of the Martian atmosphere in the UV, visible and IR spectral regions [5,6]. NOMAD has 3 channels: UVIS (ultraviolet and visible), SO (solar occultation only), and LNO (limb, nadir and occultation) covering the 200–650 nm, 2.2–4.3 μm and 2.2–3.8 μm spectral regions respectively with a spectral resolution of 1.2 nm in the UV-visible and a spectral resolution of 0.15 and 0.3 cm⁻¹ in the IR (depending on the channel). The description of the channels can be found with additional technical details in [5,28,29,33].

In the frame of this study, we have simulated spectra considering the characteristics of the SO channel for solar occultation observations and the LNO channel in case of nadir observations. These two spectrometers combine echelle gratings with high order diffraction and specific filters (acousto-optic tunable filter or AOTF) to select the spectral interval analysed by the instrument, and thus which diffraction order will be active. It results from this combination that spectra are recorded at high resolution on small spectral intervals which basically correspond to the width of the selected diffraction order (between 20 and 35 cm⁻¹).

ACS consists of three channels as well, all active in the infrared (IR) domain spanning almost the entire spectral region from 400 to 14,285 cm⁻¹ [7]. A Fourier transform spectrometer (FTS), the Thermal Infra-Red V-shape Interferometer Mounting (TIRVIM), will cover both the thermal and the mid-wave infrared spectral regions, from 400 to 5000 cm⁻¹, a mid-wave infrared channel very similar to NOMAD/SO covering the range from 2222 to 4545 cm⁻¹ (MIR), and a short-wave and near-IR channel designed to cover the 5882 to 14,285 cm⁻¹ region (SWIR and NIR). The detailed characteristics of ACS can be found in [34]. In the following, we have considered only the TIRVIM channel of ACS, which offers the highest complementarity with the NOMAD instrument.

Table 1 summarizes the specifications for the two instruments considered in this study. Note that in the case of NOMAD and ACS, both instruments have been integrated to the spacecraft and co-aligned with respect to the spacecraft axis, implying that the nadir channels will look at the same scene on the Martian surface, and that the solar occultation observations will be acquired looking at the same portion of the atmosphere. However, we do not consider here the difference which might exist in the FOV sizes and might have an impact on the signal recorded, as this is beyond the scope of the exercise described here. In the following, the two instruments will be named GA (for 'Grating with AOTF') and FTS to preserve the more general aspects of this study.

The FTS instrument, covering the entire thermal infrared spectral region and the GA spectrometer offer an interesting complementarity in both observational geometries. The broad range covered by the FTS will enable the user to retrieve surface and atmospheric temperature as well as pressure and aerosol content [35–37], and the high spectral resolution and signal-to-noise ratio (SNR) of the GA spectrometer will provide access to the

Table 1
Instrument channels considered in this study.

Instrument	GA instrument		FTS instrument	
Geometry	nadir	solar occultation	nadir	solar occultation
Type of instrument	AOTF + echelle spectrometer		Fourier transform spectrometer	
ILS	Gaussian		Sinc = sin(x)/x	
Spectral resolution	0.30 cm ⁻¹	0.15 cm ⁻¹	1.6 cm ⁻¹	0.20 cm ⁻¹
Instantaneous spectral coverage	24 cm ⁻¹	22 cm ⁻¹	Whole range	
Lower limit	2500 cm ⁻¹		400 cm ⁻¹	
Higher limit	4600 cm ⁻¹		5000 cm ⁻¹	
Signal-to-noise ratio	1000	4000	500	1000

volume mixing ratios (VMR) profile of trace species. Note that the lower resolution and SNR for observations in nadir performed by the FTS will hamper the measurement of trace gases. The values given in the Table 1 are originating from the published literature available at the time of our study. The actual observation covariance matrix S_y (assumed diagonal) is derived from the SNR values knowing the maximum amplitude of the spectra in the relevant retrieval windows. The observation vector y will be the concatenation of the corresponding spectral samples.

To retrieve trace species profiles from the NOMAD instrument, the Martian temperature profiles will be needed. In this study, we used a profile obtained through modelling (see Section 1.4). During the ExoMars mission, ACS-TIRVIM will enable temperature profile retrievals as IASI is able to retrieve reliably the telluric one [38].

Taking into account the spectral range covered by both instruments, carbon monoxide is an interesting target molecule to test synergistic retrievals. For CO, the fundamental vibrational band 1-0 and the first harmonic band 2-0 both having the ground state (GS) as lower vibrational level are used to retrieve CO respectively from spectra of the FTS and of the GA spectrometer.

At the same time, methane synergistic retrievals have been tested, using two different bands, the ν_4 band ($\nu_4=1\text{-GS}$) and the ν_3 band ($\nu_3=1\text{-GS}$). As for CO, both bands are measured by the FTS, but to test the impact of synergies, we will use the ν_4 band measured by the FTS and the ν_3 band measured by the GA spectrometer.

2.2. Spectroscopic data

Infrared spectroscopic parameters were exported from HITRAN 2012 [39] for 5 molecules: CO₂, CO, H₂O, O₃ and CH₄. However, broadening coefficients have been modified in order to account for CO₂ as the main buffer gas, whereas data reported in HITRAN are given for Earth conditions with air as the collision partner. We used broadening coefficients originating from [40–43]. Details on modifications introduced in the spectroscopic parameters line list can be found in [44].

Parameters for Rayleigh scattering were implemented from [45] and the solar irradiance data were collected from the ACE – FTS data [46] in the IR.

2.3. Selection of scenarios

The scenarios in which the synergies will be tested are defined in the following section. Different parameters are involved in this description. They are summarized in Table 2.

In order to simulate geophysical scenarios of interest, the

Martian site selected was Arabia Terra (0–40°N, 0–44°E). This particular place was chosen because the region is often mentioned as a region of interest in the search of methane [47,48], one of the species for which we tested the synergistic retrievals as well. A mid-latitude and mid-longitude region simplifies the analysis, as the seasonal cycle of condensation will not need to be considered. Nevertheless, the impact of the Martian region chosen here is not a driving factor in the analysis and we used a constant emissivity of the surface of 0.95.

Four different solar longitude (L_s) periods spanning a whole Martian year were considered: 30–60°, 120–150°, 210–240° and 300–330°. The surface temperatures (T_{surf}) at the different seasons for the chosen location are similar to one another, varying from 204 K in the winter to 216 K in the summer. Therefore the impact of the different seasons is not really significant. Solar occultation (SO) in one season only and nadir geometries in all seasons have been considered. Nadir spectra were simulated considering a position of the observing instrument at 400 km altitude and using the altitude of the surface as implemented in the 3D General Circulation Model (GCM) called Global Environment Multiscale (GEM)-Mars [49]. The orbit characteristics of ExoMars was considered with a single solar illumination (solar zenith angle of 30°). SO spectra were simulated at 14 different tangent altitudes above the surface height: + 1 km; + 3 km; from + 5 km up to + 25 km by step of 5 km, from + 27.5 km up to + 40 km by step of 2.5 km and one last at + 45 km.

Two different abundance levels for CO and CH₄ have been defined: low and high. The CO VMR were defined using the PFS measured values at the selected location and constant over the whole altitude range [13]. The values of CO VMR are 321 ppmv in the case of low VMR and of 1362 ppmv in the case of high VMR. The two different VMRs of CH₄ used were 10 and 60 ppbv, corresponding to values reported in the literature [18,19,50], the last one being possibly unrealistic according to the Curiosity measurements [51]. These values have been used to create a database of simulated spectra.

The effect of aerosols is beyond the scope of this paper and has not been taken into account in our simulations.

Table 2 summarizes the different geophysical parameters describing the chosen scenarios. They represent a total of 28 different scenarios in the solar occultation viewing mode (SO) and 8 in the nadir viewing geometry, for each instrument considered. This led to the generation of 36 theoretically simulated spectra per instrument.

2.4. Atmospheric states

The BIRA-IASB three-dimensional general circulation model (GCM) was used to provide data representative of typical atmospheric conditions of the neutral atmosphere of Mars. This includes fields such as temperature, pressure, winds and dust, as well as surface variables (e.g. temperature, pressure, CO₂ ice or water ice surface). The GEM-Mars GCM is able to reproduce the basic state of the atmosphere including the general circulation dynamics, temperature and seasonal cycles of pressure, CO₂, H₂O and O₃. The description and evaluation of the GCM can be found in [49].

In this study, global annual profiles from the surface up to 130 km were considered for temperature, pressure, CO₂, H₂O and O₃. GEM-Mars has also the capability to provide vertical profiles of dust extinction.

2.5. Simulations with ASIMUT-ALVL

All simulations of the spectra have been performed using the ASIMUT-ALVL radiative code developed at BIRA-IASB [52]. Initially

Table 2

Summary of the specifications of the selected geophysical scenarios to be simulated. The seasons are given for the Northern hemisphere. The temperature of the surface are from GEM-Mars.

Location	Arabia Terra [0–40°N; 0–44°E]
L _s (°)	30–60 (spring); 120–150 (summer); 210–240 (autumn); 300–330 (winter)
Molecules to simulate/retrieve	CO ₂ , H ₂ O, CH ₄ , CO, O ₃
CO content	low (321 ppmv)/high (1362 ppmv)
CH ₄ content	low (10 ppbv)/high (60 ppbv)
[nadir] Solar zenith angle	30°
Emission temperature of the ground for the different seasons (T _{surf})	212.23; 216.27; 211.71; 204.08 K
[SO] Tangent heights (in km above the surface)	1; 3; 5; 10; 15; 20; 25; 27.5; 30; 32.5; 35; 37.5; 40; 45
Blackbody temperature of the incoming solar spectrum	5780.0 K

developed for Earth observation missions (IASI and ACE-FTS), the code was later adapted for planetary atmospheres, in particular for Venus [44] and Mars [53]. ASIMUT-ALVL is a modular program for radiative transfer calculations in planetary atmospheres. This code has been developed with the objective to be as general as possible, accepting different instrument types (Fourier transform spectrometers, grating spectrometers, AOTF combined with an echelle grating) and different geometries (nadir, ground-based, solar occultation/limb). The different radiation contributions such as the Sun contribution (direct or reflected on the surface), the surface emission contribution and the thermal atmospheric emission contribution are taken into account. More details about this algorithm can be found on the website of BIRA-IASB (http://planetary.aeronomie.be/en/asimut_documentation/html/index.html). In the following paper, the expressions “pass” and “FEN” will be often used. The passes represent the different steps during the retrieval process. FEN is the acronym for “fenêtre” which means “window” in French. The FEN represent the different spectral windows used to perform the retrieval.

To obtain a statistically representative sample, random noise figures have been added to the 36 (28+8) simulated spectra. Sets of 50 spectra were created in nadir and 10 in solar occultation for each of the scenarios. This led to a dataset of 680 (28 × 10 + 8 × 50) spectra for each instrument considered. Examples of these spectra are shown in Fig. 1 and Fig. 2.

Fig. 1 shows typical FTS spectra for nadir observation. Note the wide spectral range covered by the Fourier transform technique. However, this is at the cost of a lower spectral resolution as compared to GA measurements. In Fig. 2, GA spectrometer spectra simulated in solar occultation geometry are presented. The spectral range is narrower but the resolution is higher. Both instruments are therefore complementary to one another.

3. Retrievals

ASIMUT-ALVL has been used to perform the retrievals as well. The main retrieval module is based on the optimal estimation method (OEM) [54] coupled to the analytical calculation of the Jacobians. This code allows to fit simultaneously or sequentially different parts of one or more spectra, to fit the surface temperature, T_{surf} , to fit column/vertical profiles for molecular species and for aerosols and to fully characterize the outputs (averaging kernels, errors, degree of freedom, etc.).

3.1. Methodology

Retrievals have been performed on 680 spectra simulated as described in the previous sections. In order to test the impact of the synergies, 4 different types of runs have been executed:

- In non-synergy:
 - Retrievals from “GA only” spectra
 - Retrievals from “FTS only” spectra
- In synergy:
 - Level 1/ Level 1 (L1/ L1) retrievals combining FTS and GA spectra in the same retrieval
 - Level 2/Level 1 (L2/L1) retrievals combining sequentially the retrieved information from one instrument with the spectra from the other one.

Here, L1 data represent calibrated spectra recorded by one of the instruments, while L2 data are physical quantities retrieved from one spectrum or one set of spectra (temperature, VMR profiles, etc.). It is important to define precisely how the synergies occur. To perform a L1/L1 synergy, ASIMUT-ALVL will consider the spectra from both instruments simultaneously and retrieve the molecular abundances from both of them considered together, i.e. information will be extracted from the two sets of spectra during the same retrieval procedure.

In the case of the L2/L1, the choice was made to use the FTS spectra in a first pass to retrieve the CO₂ and H₂O VMR profiles, as well as the surface temperature (T_{surf}) in nadir taking advantage of the broad spectral range offered by this instrument. In a second pass, the data obtained during the first pass will be used as input and CO and CH₄ VMR profiles will then be retrieved from the GA spectrometer spectra only, taking advantage of the higher spectral resolution and SNR of this latter instrument. The runs have been performed starting from spectra simulated with the same *a priori* profiles (considered as the truth) as described in the next section. Depending on the geometry, the first guess profile was chosen randomly for solar occultation and fixed for nadir observations. The VMR profiles, errors, averaging kernels and degree of freedom for signal (DOFS) values are available for comparison, and help to conclude on the impact of this method. The averaging kernels (AK) are obtained and represent the sensitivity to the true state. Their utilisation enables us to determine the level of information available along the altitude range. The degree of freedom for signal (DOFS) is mathematically the trace of the AK matrix. It indicates the number of pieces of information that can be retrieved independently.

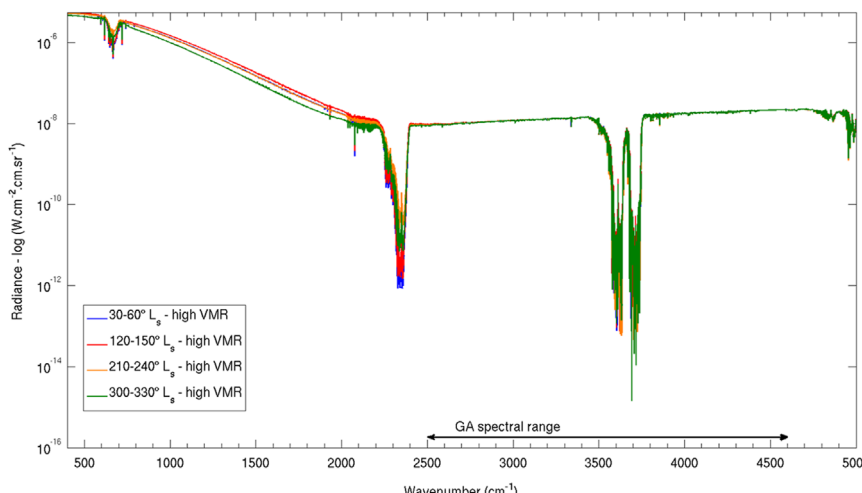


Fig. 1. Simulated FTS spectra in nadir with ASIMUT-ALVL for high VMR of CO and CH₄ at 4 different L_s periods. The radiance is given in logarithmic scale. The black double arrow indicates the GA instrument's spectral range.

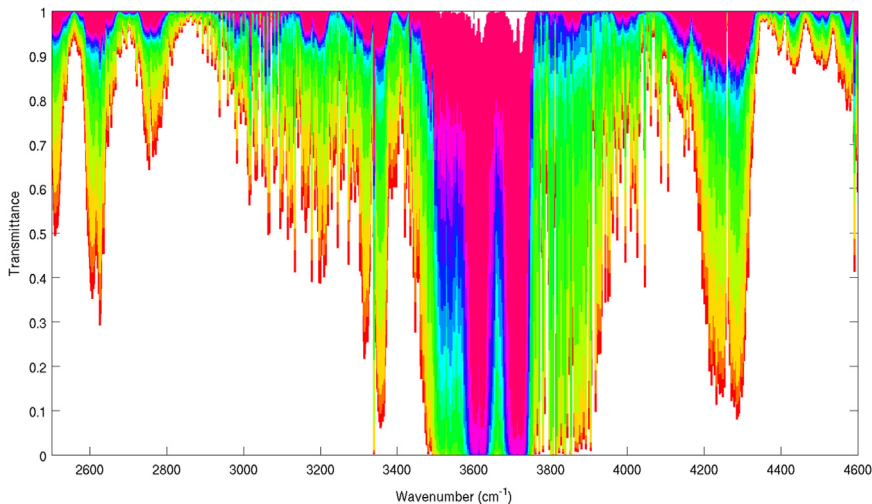


Fig. 2. Simulated GA spectrometer spectra in solar occultation with ASIMUT-ALVL for high VMR of CO and CH₄ at 14 different tangent altitudes during the same L_s period. Each color corresponds to one altitude, the red being the lowest (1 km) and the pink the highest (45 km). (For interpretation of the references to color in this figure legend, the reader is referred to the web version of this article.)

Taking into account the level of information available, we retrieved the vertical column densities in the case of nadir observations and vertical VMR profiles in the case of solar occultation observations. In particular, the retrieval in solar occultation will take into account the entire set of occultation spectra and not each spectrum in sequence, i.e. in the SO case, the 14 spectra (one for each altitude) are considered altogether in the case of non-synergy and 28 spectra are considered altogether in the case of L1/L1 synergy (14 for each instrument). In the case of L2/L1, the 14 spectra of the FTS are considered in the first pass then the 14 ones of the GA spectrometer are used in the second pass.

3.2. *A priori* profiles

To perform the retrievals, ASIMUT-ALVL needs an *a priori* atmospheric profile for each physical quantity:

1. The altitude scale as well as the pressure and temperature profiles were not modified from the ones used for the simulations, i.e. they correspond to the profiles delivered by the GEM-Mars model.
2. No O₃ retrieval was performed. This molecule was only simulated using the GEM-Mars profiles.
3. The first guess profiles for CO₂ and H₂O have the same shape as the *a priori* calculated GEM-Mars profiles, but are scaled by a multiplicative factor of 0.9 in order to check the efficiency of the algorithm to converge to the right solution (the true one being the GEM-Mars profiles used to simulate the input spectra).
4. In the case of nadir retrievals, we defined a vertically constant first guess profile using an average VMR between the high VMR values and the low VMR ones i.e. 35 ppbv for CH₄ and 841.5 ppmv for CO.
5. In the case of solar occultation retrievals, we used a random first guess profile scaled ($\pm 5\%$ at the 1σ level) around the CH₄ or CO *a priori* profiles of GEM-Mars, i.e. the ones used for the simulation.

3.3. Selection of the spectral ranges

The two instruments considered in this study may share common planetary objectives but will definitely operate differently. On the one hand, the FTS covers a broad spectral range with a moderate SNR, and low resolution in nadir whereas on the other

hand, the grating spectrometer coupled to an acousto-optic filter for order selection [5], will record spectral intervals (diffraction orders) with a width of 20 to 35 cm⁻¹ at high resolution and high SNR. The specifications of the channels of interest for this study were summarized in Table 1.

The approach adopted here is to remain as close as possible to the expected characteristics of the measurements. So the corresponding spectral ranges will therefore differ from one instrument to another.

The spectral range of the GA spectrometer spans the 2500 to 4600 cm⁻¹ domain and covers the following vibrational bands:

- the 2-0 band of CO centered at 4347 cm⁻¹;
- the ν_3 band of CH₄ centered at 3019 cm⁻¹.

This grating spectrometer cannot measure the entire band during one observation. Indeed, because the diffraction orders cover a limited wavenumber range, a specific signature (full molecular band, P-Q-R-branches) may not be recorded entirely in one single spectrum. From our experience with the SOIR instrument [55], for the actual NOMAD instrument we will specify which order of diffraction (spectral window) will offer the most useful information to retrieve target molecular species such as CO₂, H₂O, CO and CH₄. A parallel study to determine the detection limits of trace species was performed independently of the present work, giving us access to the best diffraction orders to be used for the analysis of the Martian atmosphere with NOMAD [56].

The spectral range of the FTS instrument being very wide (400 to 5000 cm⁻¹), two bands of CO can be covered at once: the 1-0 and the 2-0 and two bands of CH₄ as well: ν_4 and ν_3 . For the sake of this study, we have chosen to retrieve CO abundances from the FTS regions not accessible to the GA instrument, in order to gain insight on the impact of synergies. For the FTS, we therefore used:

- the 1-0 band of CO centered at 2143 cm⁻¹;
- the ν_4 band of CH₄ centered at 1306 cm⁻¹.

But since it is not practical to consider the complete FTS range during one single retrieval, we have limited the useful spectral range to appropriate smaller windows.

Finally, to perform the retrievals discussed in this study, the algorithm was parameterized such that CO₂, H₂O, CO and CH₄ are fitted in the selected spectral regions given in Table 3. Ozone is

Table 3

Spectral ranges used to retrieve molecular abundances.

	FEN1 (cm^{-1})	FEN2 (cm^{-1})	FEN3 (cm^{-1})	FEN4 (cm^{-1})	FEN5 (cm^{-1})
FTS nadir (SP1)	1094–1230 surface temperature	2000–2250 CO_2, CO	3500–4050 $\text{CO}_2, \text{H}_2\text{O}$	1200–1400 $\text{CO}_2, \text{H}_2\text{O}, \text{CH}_4$	500–800 $\text{CO}_2, \text{H}_2\text{O}$
GA nadir (SP2)	3016–3041 $\text{CO}_2, \text{H}_2\text{O}, \text{CH}_4$	3105–3131 $\text{CO}_2, \text{H}_2\text{O}, \text{CH}_4$	4267–4302 $\text{CO}, \text{H}_2\text{O}$	2591–2613 $\text{CO}_2, \text{H}_2\text{O}$	
FTS SO (SP1)	2000–2250 CO_2, CO	3800–4100 $\text{CO}_2, \text{H}_2\text{O}$	1200–1400 $\text{CO}_2, \text{H}_2\text{O}, \text{CH}_4$	500–650 $\text{CO}_2, \text{H}_2\text{O}$	1456–1796 H_2O
GA SO (SP2)	3011–3037 $\text{CO}_2, \text{H}_2\text{O}, \text{CH}_4$	3056–3082 $\text{CO}_2, \text{H}_2\text{O}, \text{CH}_4$	4248–4305 $\text{CO}, \text{H}_2\text{O}, \text{CO}_2$	3349–3376 $\text{CO}_2, \text{H}_2\text{O}$	3798–3830 $\text{CO}_2, \text{H}_2\text{O}$

only simulated, i.e. not retrieved to avoid any additional uncertainty due to the poor constraint (from the observed spectra) on this species.

The spectral windows given in Table 3 were used as such in the case of non-synergy.

In the cases of synergies, we used the same windows but in combination:

- For the L1/L1 synergy in nadir, the 5 windows of SP1 (FTS nadir) and the 4 windows of SP2 (GA nadir) were used simultaneously (see Table 3), representing 9 fitted windows overall.
- For the L2/L1 synergy in nadir, we used 3 spectral windows for SP1 (FTS nadir) i.e. FEN1, FEN3 and FEN5, followed by the fit of 3 windows of SP2 (GA nadir) namely FEN1, FEN2 and FEN3, representing 6 fitted windows in total.
- For the L1/L1 synergy in SO, the 10 windows of Table 3 could not be used altogether for the 28 (14+14) occultation spectra of the 2 instruments due to excessive computation time. A selection was made such as to use the best spectral windows and to remain efficient timewise. The 2 windows FEN1 and FEN3 of SP1 (FTS SO) as well as the 3 windows FEN1, FEN2 and FEN3 of SP2 (GA SO) were used simultaneously (5 windows in total).
- For the L2/L1 synergy in SO, we used 3 windows of SP1 (FTS SO) i.e. FEN2, FEN4 and FEN5 followed by the fit of 3 windows of SP2 (GA SO) i.e. FEN1, FEN2 and FEN3 (6 windows in total).

3.4. Impact of the different synergies

Four different types of runs were performed on the noisy spectra (50 in nadir and 10 in solar occultation) for each scenario, two for each instrument separately and two for each synergy type. In each run 4 molecules have been retrieved: CO_2 , H_2O , CO and CH_4 .

There are two different kinds of fit possible with ASIMUT-ALVL. Retrievals of molecular abundances can be done in "column" or in vertical "profile" modes. In the "column" mode, ASIMUT-ALVL will not modify the shape of the vertical VMR input profile (the first guess profile). It will only adjust the VMR values using a scaling coefficient on the whole altitude range of the profile. In the vertical "profile" mode, ASIMUT-ALVL will be free to fit each point of the altitude range according to the spectral information available in the complete set of input spectra. We decided to use the "column" mode in the nadir geometry and the "profile" mode in the solar occultation geometry. These choices will be justified in the next two sections, which are based on typical retrievals results. For the nadir geometry, we verified that the abundance of molecules retrieved in the "column" mode is equivalent (within the error

bars) to the column derived from the retrieved vertical "profile" in the profile mode.

3.4.1. Nadir retrievals

A total number of 400 runs has been performed for the nadir case. We discuss the results obtained in this section for CO and for CH_4 separately.

In the case of nadir, we used the "column" mode retrieval, since the degree of freedom and averaging kernels in the vertical "profile" mode are not satisfactory to retrieve a full molecular VMR profile, as shown on Fig. 3. At high altitude, no information is available in the spectra to constrain the inversion, as shown by the averaging kernels (AK in the 3rd line). Therefore, the vertical profile obtained follows the *a priori* profile (in pink) between 50 and 150 km, as can also be seen on the retrieved profiles (1st line). At lower altitudes, the fit reaches the true solution (green line), exceeding at some altitudes the GEM-Mars value (to compensate the bad fit at high altitudes) since below 50 km some information is potentially available in the spectra to retrieve a profile. However the retrieved solution is biased and the profile obtained is generally away from the expected true solution (in red). This test-case shows the difficulty to retrieve a vertical profile of trace species from nadir measurements (a situation also known for nadir sounding of the Earth atmosphere [57]).

In Fig. 3, the mode of the retrieval was set as "profile". The plots on the upper panels are the vertical profiles of VMR for each fitted species (from left to right: CH_4 , CO , H_2O and CO_2). The first guess is represented in pink and the true solution in green. In blue are represented the retrieved values, in plain the value itself and in dotted line the error bar. The second panel represents the variability matrix (diagonal terms) which has been set to 10%. The averaging kernels (AK) are plotted together with an indication of the value of the DOFS in the plots of the third line. The DOFS values indicate here that only 1 piece of information (or not even in the case of CH_4) can be retrieved independently. Finally, the plots on the bottom panel represent the *a priori* covariance \mathbf{S}_a and the *a posteriori* error matrices (diagonal terms) with \mathbf{S}_m the measurement error covariance, \mathbf{S}_{sm} the smoothing error and \mathbf{S}_{tot} the total error (on the retrieved state vector \mathbf{x}).

We computed the spectrum over the entire spectral range using the retrieved quantities via both fitting methods. Fig. 4 shows the simulation of the entire spectral range using the retrieved quantities when fitted in the "column" mode (in red) and in vertical "profile" mode (in dark blue). As seen in the figure, the error is smaller in the case of a "column" mode retrieval. This is seen also in the lower panel showing the difference between observed (here the input spectrum simulated with noise) and spectra calculated using the retrieved parameters at the end of the iteration process.

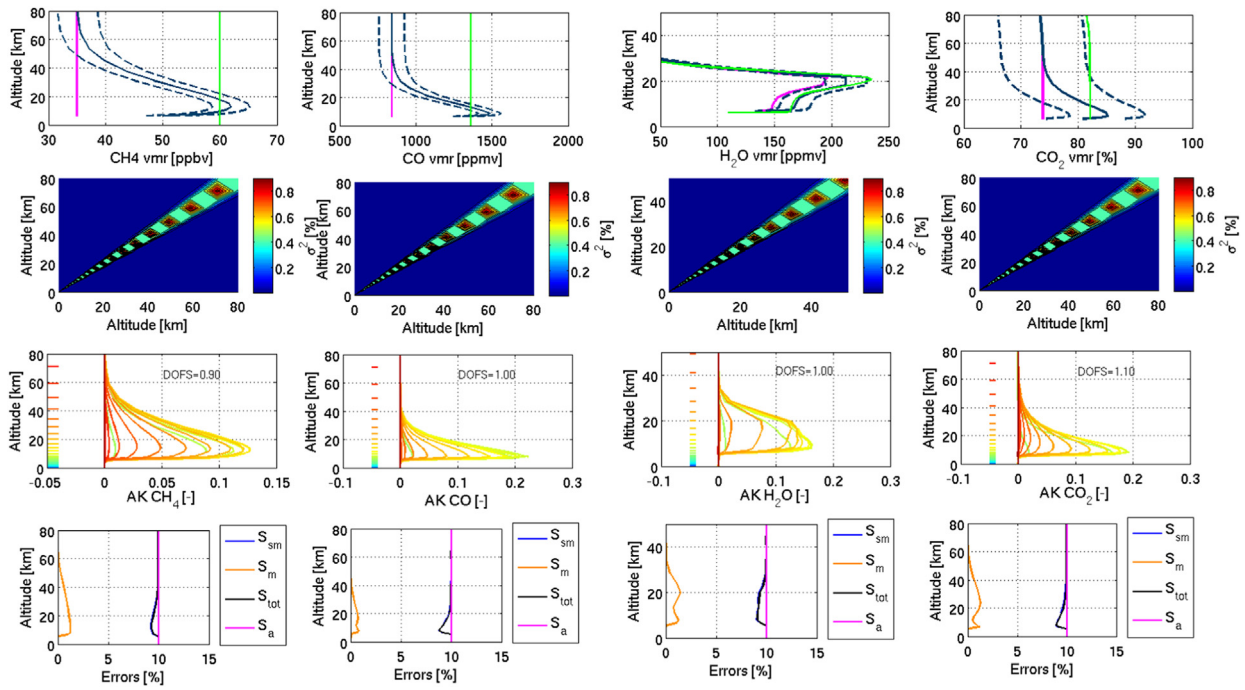


Fig. 3. Retrieved profiles obtained with ASIMUT-ALVL in the case of $L_s=30\text{--}60^\circ$, high VMR and no aerosol for the GA instrument in nadir mode (See text for more information). (For interpretation of the references to color in this figure legend, the reader is referred to the web version of this article.)

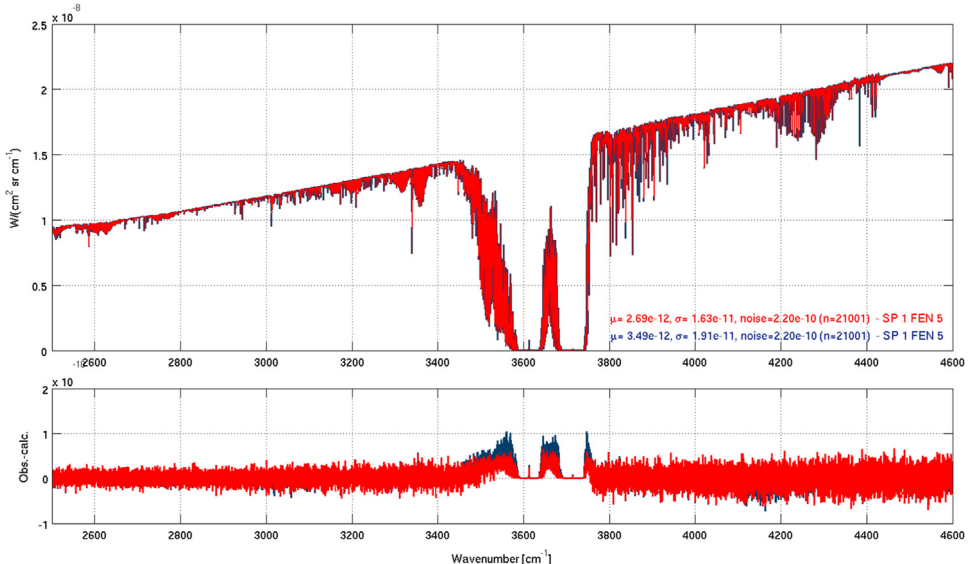


Fig. 4. Comparison of different fitted spectra with one simulated observation in the nadir mode, on the whole spectral range of the GA spectrometer. The two fitted spectra (not easily distinguishable in the upper panel) correspond to the retrievals in “column” (red) and in “profile” (dark blue) modes. The differences between observed and calculated spectra for each method are given in the lower panel. The noise value of the spectrum is 2.20×10^{-10} (in radiance units). (For interpretation of the references to color in this figure legend, the reader is referred to the web version of this article.)

The mean value of (observed – calculated), given by μ and the standard deviation of (observed – calculated), given by σ (see legend on Fig. 4) are both smaller in the case of the column mode retrieval, as is the (observed-calculated) given in the lower panel. This confirmed the choice of retrieving abundances in nadir using vertical column mode only.

a) CH₄ retrieval

Results of all the retrievals of methane are shown in the following figures. Fig. 5 and Fig. 6 illustrate the results when no synergy is considered. The two panels represent the low VMR case

on the left and the high VMR case on the right. The 4 L_s periods are represented using different colors. The figures represent the statistical distribution of the 50 retrieved abundances. In each panel, the black line indicates the VMR profile used to simulate the spectra (“the truth” or true solution, see Table 2 for the values). The markers in color in the middle of the bin represent the number of retrievals leading to a VMR value, in the bins considered. The width of the bins is given in the captions. The colored horizontal dotted lines at each marker represent the mean error on the retrievals considered in the bin. The first guess value used for these runs was a constant profile of 35 ppbv for both concentration cases, not shown on the plots. The mean retrieved abundance at

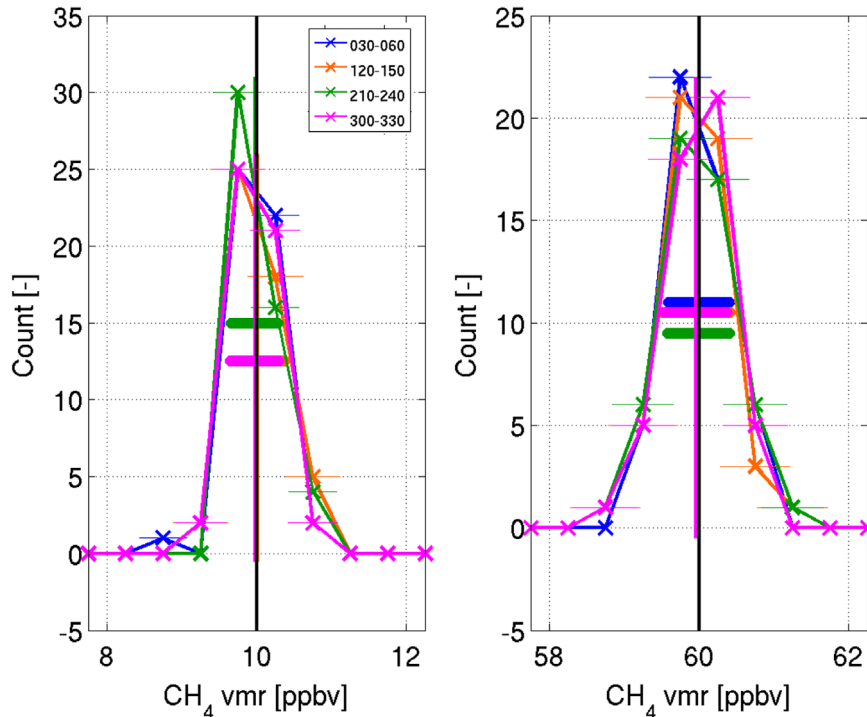


Fig. 5. Statistical distribution of the 50 retrievals (in the column mode) of CH_4 with the GA instrument in the nadir mode in the case of low VMR (10 ppbv) on the left and high VMR (60 ppbv) on the right. The four different L_s periods are indicated in different colors. The first guess value was 35 ppbv in all cases and is not shown on the plots. All results within 0.5 ppbv are binned together. The black vertical line on each plot represents the GEM value expected to be retrieved. The colored vertical line indicates the mean abundance at each season with their respective error bar. (For interpretation of the references to color in this figure legend, the reader is referred to the web version of this article.)

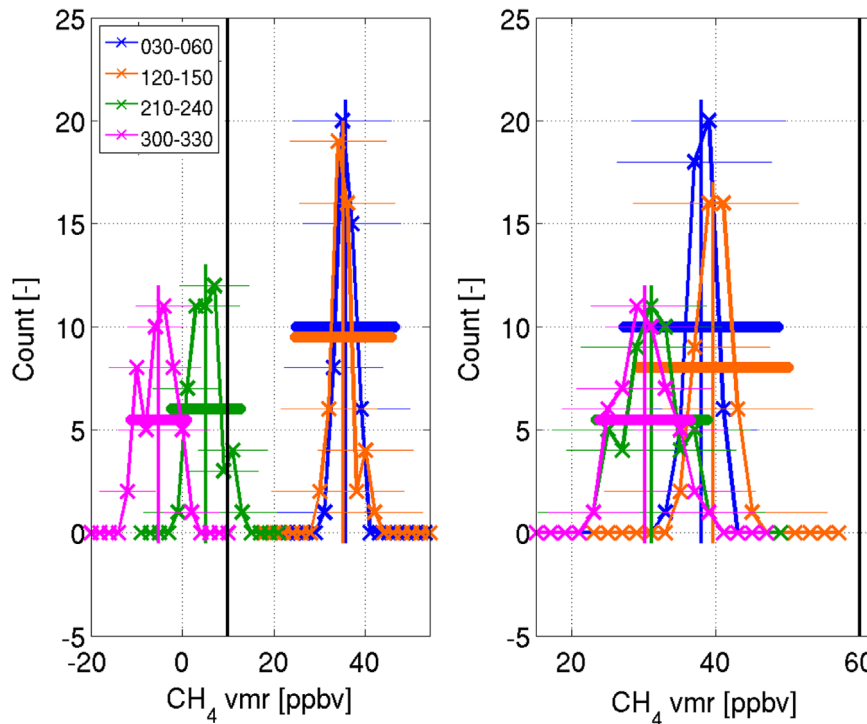


Fig. 6. Statistical distribution of the 50 retrievals (in the column mode) of CH_4 with the FTS instrument in the nadir mode in the case of low VMR (10 ppbv) on the left and high VMR (60 ppbv) on the right. The four different L_s periods are indicated in different colors. The first guess value was 35 ppbv in all cases and is not shown on the plot. All results within 2 ppbv are binned together. The black vertical line on each plot represents the GEM value expected to be retrieved. The colored vertical line indicates the mean abundance at each season with their respective error bar. (For interpretation of the references to color in this figure legend, the reader is referred to the web version of this article.)

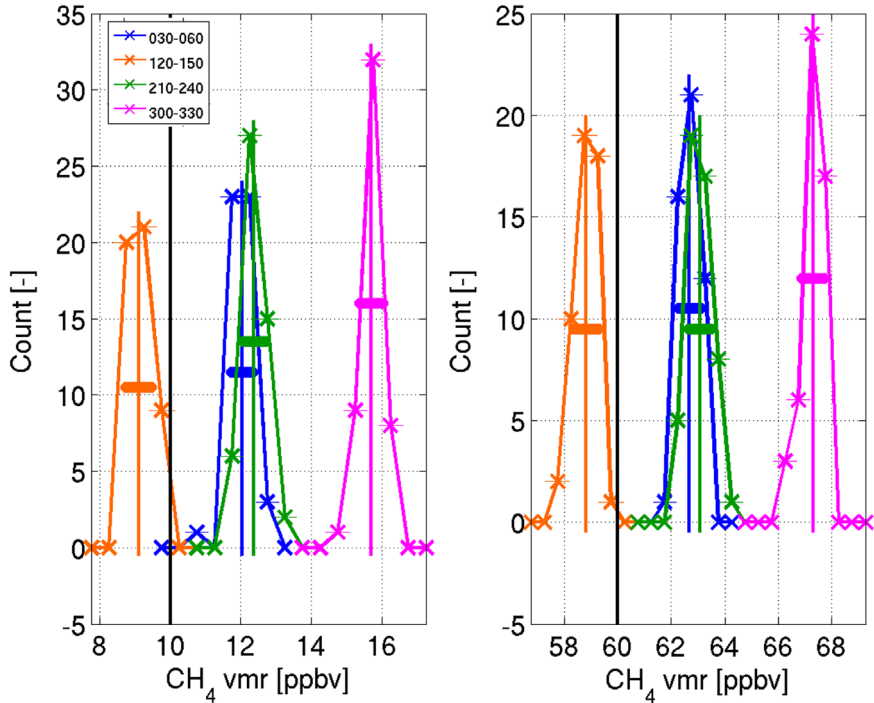


Fig. 7. Statistical distribution of the 50 retrievals (in the column mode) of CH_4 in the L1/L1 synergy case in the nadir mode with a low VMR (10 ppbv) on the left and a high VMR (60 ppbv) on the right. The four different L_s periods are indicated in different colors. The first guess value was 35 ppbv in all cases and is not shown on the plots. All results within 0.5 ppbv are binned together. The black vertical line on each plot represents the GEM value expected to be retrieved. The colored vertical line indicates the mean abundance at each season with their respective error bar. (For interpretation of the references to color in this figure legend, the reader is referred to the web version of this article.)

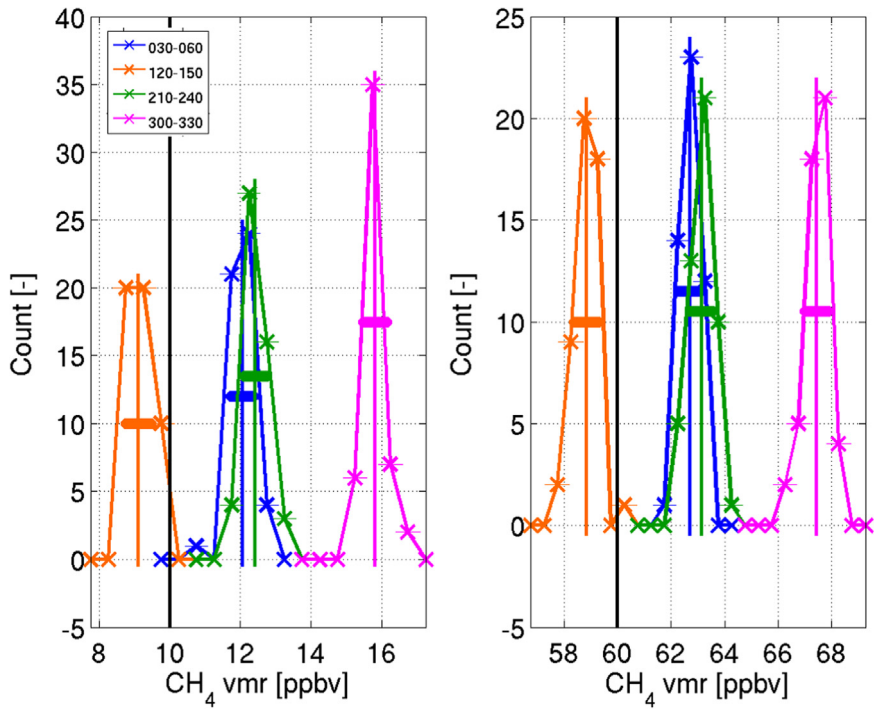


Fig. 8. Statistical distribution of the 50 retrievals (in the column mode) of CH_4 in the L2/L1 synergy case in the nadir mode with a low VMR (10 ppbv) on the left and a high VMR (60 ppbv) on the right. The four different L_s periods are indicated in different colors. The first guess value was 35 ppbv in all cases and is not shown on the plots. All results within 0.5 ppbv are binned together. The black vertical line on each plot represents the GEM value expected to be retrieved. The colored vertical line indicates the mean abundance at each season with their respective error bar. (For interpretation of the references to color in this figure legend, the reader is referred to the web version of this article.)

each season is represented as a vertical line in the associated color. The thick horizontal error bar indicates the mean error on the 50 retrieved VMR. For the “GA only” runs, the VMR values retrieved are obtained with a 0.7% uncertainty in the case of high VMR and

3.0% in the case of low VMR, as can be seen in the Table 4.

The results are very similar for all seasons in the case of GA (Fig. 5) while in the case of the FTS (Fig. 6), the retrievals values are grouped in two cases. As discussed earlier, the surface temperature

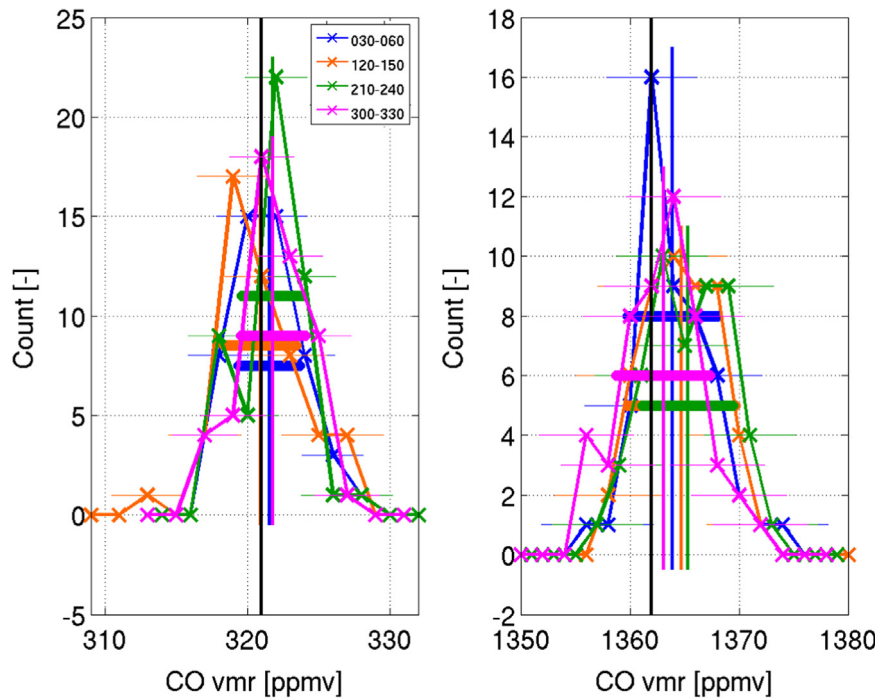


Fig. 9. Statistical distribution of the 50 retrievals (in the column mode) of CO with the GA instrument in the nadir mode in the case of low VMR (321 ppmv) on the left and high VMR (1362 ppmv) on the right. The four different L_s periods are indicated in different colors. The first guess value was 841.5 ppmv in all cases and is not shown on the plots. All results within 2 ppmv are binned together. The black vertical line on each plot represents the GEM value expected to be retrieved. The colored vertical line indicates the mean abundance at each season with their respective error bar. (For interpretation of the references to color in this figure legend, the reader is referred to the web version of this article.)

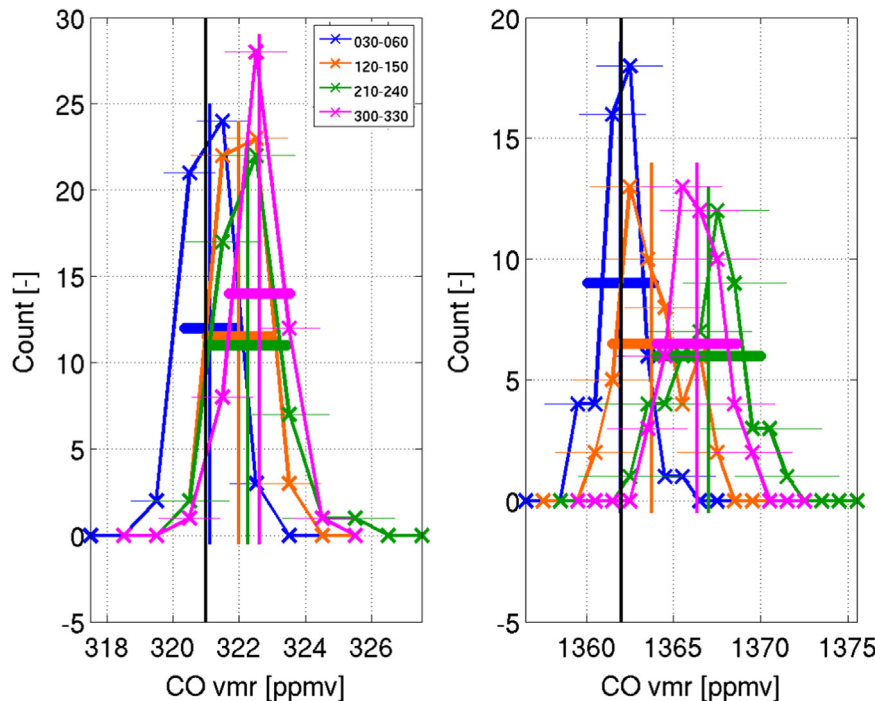


Fig. 10. Statistical distribution of the 50 retrievals (in the column mode) of CO with the FTS instrument in the nadir mode in the case of low VMR (321 ppmv) on the left and high VMR (1362 ppmv) on the right. The four different L_s periods are indicated in different colors. The first guess value was 841.5 ppmv in all cases and is not shown on the plots. All results within 1 ppmv are binned together. The black vertical line on each plot represents the GEM value expected to be retrieved. The colored vertical line indicates the mean abundance at each season with their respective error bar. (For interpretation of the references to color in this figure legend, the reader is referred to the web version of this article.)

during these different periods are not very different (see Table 2), implying a weak seasonal effect on the results.

As can be seen in Fig. 6, the profiles for the “FTS only” do not match the true solution, even for the high VMR conditions. Indeed,

the fitted profiles are largely spread around the *a priori* value, even reaching non-physical (negative) VMR in the low concentration case. This is due to the fact the ν_4 band covered in this retrieval is a weak feature in the Martian spectra (very small abundance of CH₄

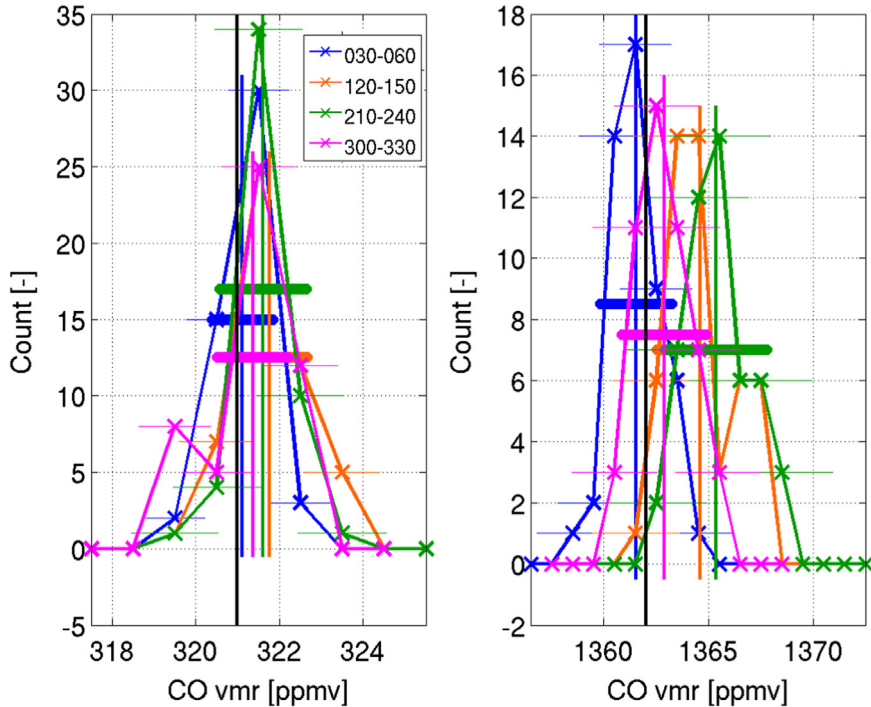


Fig. 11. Statistical distribution of the 50 retrievals (in the column mode) of CO in the L1/L1 synergy case in the nadir mode with low VMR (321 ppmv) on the left and a high VMR (1362 ppmv) on the right. The four different L_s periods are indicated in different colors. The first guess value was 841.5 ppmv in all cases and is not shown on the plots. All results within 1 ppmv are binned together. The black vertical line on each plot represents the GEM value expected to be retrieved. The colored vertical line indicates the mean abundance at each season with their respective error bar. (For interpretation of the references to color in this figure legend, the reader is referred to the web version of this article.)

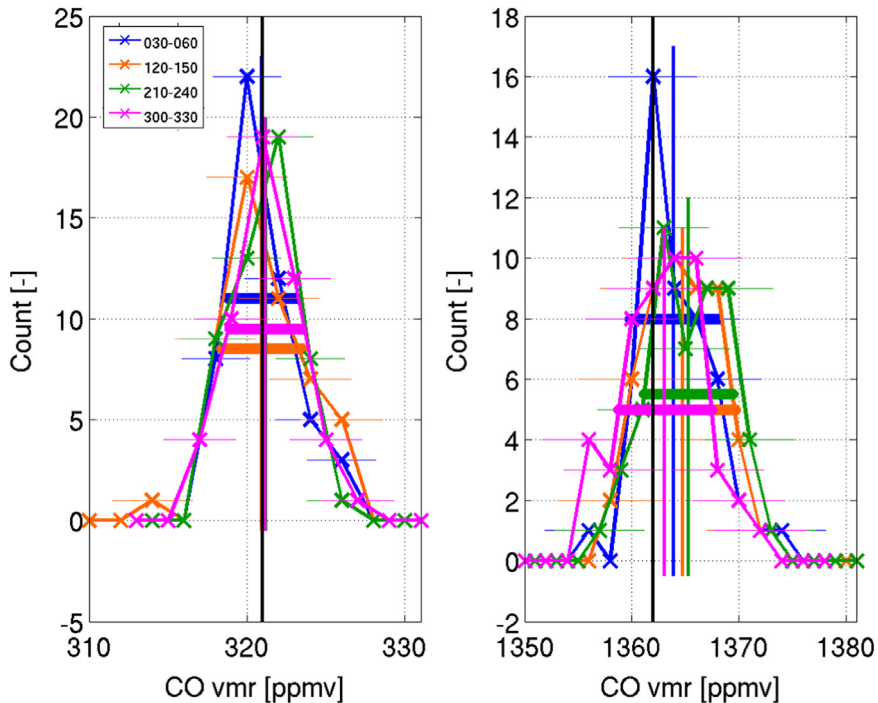


Fig. 12. Statistical distribution of the 50 retrievals (in the column mode) of CO in the L2/L1 synergy case in the nadir mode with low VMR (321 ppmv) on the left and a high VMR (1362 ppmv) on the right. The four different L_s periods are indicated in different colors. The first guess value was 841.5 ppmv in all cases and is not shown on the plots. All results within 2 ppmv are binned together. The black vertical line on each plot represents the GEM value expected to be retrieved. The colored vertical line indicates the mean abundance at each season with their respective error bar. (For interpretation of the references to color in this figure legend, the reader is referred to the web version of this article.)

and FTS instrument noise combined with low spectral resolution). This is explaining why the degree of freedom for signal (DOFS) equals 0.1. This ν_4 band of CH_4 should not be considered as a good

candidate to retrieve the methane abundance with the FTS, whereas the stronger ν_3 band targeted by the GA instrument enables a successful fit. Both bands are presented in transmittance

in Fig. 13 and Fig. 14. Note that we have not investigated the possibility for the FTS instrument to retrieve information on methane using the ν_3 band, since what we wanted to prove or underline is the usefulness of considering complementary information.

Unfortunately for methane, the synergy between the two instruments FTS and GA cannot overcome the impact of the unsuccessful retrieval using the ν_4 band alone (only covered by the FTS). Fig. 7 and Fig. 8 show the results for CH₄ synergistic retrieval using either the L1/L1 or the L2/L1 synergy. The results in both synergies appear to be very similar. The DOFS is 1.0 in both cases and the inversions are successful even if the retrieved profiles are not fully recovering the "truth". As can be seen in Table 4, the runs using the "GA only" spectra are the closest to the true solution, with the smallest error bars.

The seasonal trends are similar in the case of the synergistic retrievals. The warmer the surface, 216 K in the summer, the stronger the signal is in the TIR spectral region, the closer the retrieval is to the solution.

b) CO retrieval

The CO retrievals with the GA instrument were performed using the 2-0 band in a spectral window of 35 cm⁻¹ width, i.e. between 4267 and 4302 cm⁻¹. The CO retrievals with the FTS instrument were done using the 1-0 band in a spectral window 250 cm⁻¹ wide, between 2000 and 2250 cm⁻¹. We have chosen to perform the retrievals in the column mode for the reasons explained at the beginning of the section (lack of sensitivity of nadir sounding with respect to the shape of the profile).

A number of 50 noisy spectra was used in each scenario. They give similar results, as can be seen in Fig. 9 and Fig. 10. The distribution of the results are represented by the colored markers in bin of 1 or 2 ppmv. Errors are also given, as dotted horizontal colored lines in the figures. The results are shown for all 4 L_s periods. There is no significant seasonal trends. The retrievals using the GA instrument are matching well the black vertical line, i.e. the true solution profile, within the error bars which reach 0.3% and 0.7% in the case of high and low VMR respectively. The retrievals using the FTS instrument are centered around the true solution for the spring case for both concentrations (in blue) while the summer case (in orange - highest T_{surf}) CO retrievals are successful (i.e. matching the "truth") in high concentration only and the retrievals done when the surface temperatures are the lowest (autumn (in green) and winter (in magenta)) are not exactly reaching the solution in neither cases. On the other side, we conclude that the differences of T_{surf} for each season are too small to be relevant. The mean retrieved values of volume mixing ratios are given in the Table 5.

In the case of CO, the synergies offer interesting results. Both retrievals (L1/L1 and L2/L1) were successful as can be seen in Fig. 11 and Fig. 12. The spectral information available is sufficient and the true solution is reached. Again the DOFS are equal to 1.0.

No seasonal trend can be highlighted.

In particular, the synergy L1/L1 benefits from both spectra and from the information contained in both bands of CO measured by the instruments. This is confirmed by the retrieved VMR values and their *a posteriori* uncertainties shown in Table 5. The L1/L1 synergy profile is still very near the true solution and presents the smallest error bars at each season.

3.4.2. Solar occultation retrievals

In the case of solar occultation spectra, the molecular VMR profiles were retrieved from 14 spectra representing one representative occultation, spanning the altitude range from 1 to 45 km above the surface (defined in the GCM GEM-Mars). Some differences from the nadir study are worth to be highlighted. First, enough information is available in the spectra to derive a vertical profile and not only a column, as will be shown in the two next sections. Secondly, no access to the surface temperature is possible in this geometry. Thirdly, the results will not easily compare to the observations/simulations, as the total column over the entire altitude range is not a good representation of the solar occultation results (only sampling the profile down to ~7 km). And finally, a practical difference has to be mentioned: the runs are more time-consuming, especially for the L1/L1 synergy, as 28 spectra have to be fitted in one single pass.

For testing the robustness of the retrieval, we have chosen to select 10 noise realizations perturbing the simulated spectrum calculated from the "true" profile, each of them associated with a first guess vertically constant profile varying randomly around 95% to 105% of the true value. This procedure has been applied both for CH₄ and CO.

In the case of solar occultation, only one season (L_s = 30–60°) was considered. As the source of the signal is the sunlight and as no thermal emission from the surface will contribute, no seasonal impact is expected in this geometry of observation.

In the next sections, we will describe in more detail the results obtained for CH₄ and CO, but some main results can already be discussed here. The retrieved vertical profiles all present some fluctuations which can be easily seen in Fig. 15, Fig. 16, Fig. 18 and Fig. 19 (note that the horizontal scale is expanded around the values of interest). This is a behaviour which is often observed with the OEM method, and in some cases a Tikhonov approach [58] is applied to reduce them. We did not do this here for two reasons: (1) we want to compare results from the different cases (with and without synergies) obtained in exactly the same way, and (2) we believe that those fluctuations reflect the basic properties of the OEM. We tried different approaches to check that their amplitudes are consistent with the retrieval hypotheses by constraining more/less the inversion by changing the variance of the *a priori* state vector (S_a matrix, uncertainty ranging from 1% to 99%), by adding non-diagonal elements in the S_a matrix (the atmospheric layers are in fact not independent) and varying the length of mixing between the layers. However, we did not want to change the SNR values as it is often (wrongly) done in OEM, since

Table 4

CH₄ mean abundances retrieved in the nadir mode.

L _s	True VMR (ppbv)	GA (ppbv)	FTS (ppbv)	Both instruments - L1/L1 (ppbv)	Both instruments - L2/L1 (ppbv)
30–60°	10	9.98 ± 0.31	35.60 ± 10.71	12.04 ± 0.32	12.05 ± 0.32
120–150°	10	10.02 ± 0.37	35.18 ± 10.45	9.11 ± 0.36	9.12 ± 0.36
210–240°	10	9.98 ± 0.32	5.09 ± 7.52	12.37 ± 0.32	12.43 ± 0.32
300–330°	10	9.98 ± 0.33	-5.16 ± 6.07	15.70 ± 0.34	15.82 ± 0.34
30–60°	60	60.00 ± 0.41	37.95 ± 10.70	62.69 ± 0.42	62.70 ± 0.42
120–150°	60	59.96 ± 0.46	39.62 ± 10.44	58.83 ± 0.46	58.84 ± 0.46
210–240°	60	60.00 ± 0.41	31.08 ± 7.73	63.07 ± 0.42	63.14 ± 0.42
300–330°	60	59.96 ± 0.42	30.13 ± 6.35	67.29 ± 0.44	67.43 ± 0.44

Table 5

Average values of the CO volume mixing ratio obtained in the different scenarios and synergies (non-synergistic or synergistic) for the nadir mode. For easier comparison the non-synergistic retrievals (columns 2 and 3) are presented together with the synergistic retrievals (columns 4 and 5).

L_s	True VMR (ppmv)	GA (ppmv)	FTS (ppmv)	Both instruments L1/L1 (ppmv)	Both instruments L2/L1 (ppmv)
30°-60°	321	321.53 ± 2.15	321.13 ± 0.77	321.11 ± 0.73	320.93 ± 2.15
120°-150°	321	320.91 ± 2.56	321.99 ± 0.96	321.76 ± 0.90	320.95 ± 2.56
210°-240°	321	321.77 ± 2.17	322.26 ± 1.19	321.62 ± 1.04	321.20 ± 2.17
300°-330°	321	321.80 ± 2.27	322.62 ± 0.92	321.36 ± 0.85	321.18 ± 2.26
30°-60°	1362	1363.94 ± 4.12	1361.95 ± 1.89	1361.53 ± 1.72	1363.95 ± 4.12
120°-150°	1362	1364.74 ± 4.95	1363.77 ± 2.30	1364.62 ± 2.08	1364.74 ± 4.95
210°-240°	1362	1365.30 ± 4.16	1367.03 ± 2.97	1365.36 ± 2.42	1365.35 ± 4.16
300°-330°	1362	1363.06 ± 4.33	1366.34 ± 2.29	1362.87 ± 2.02	1363.11 ± 4.33

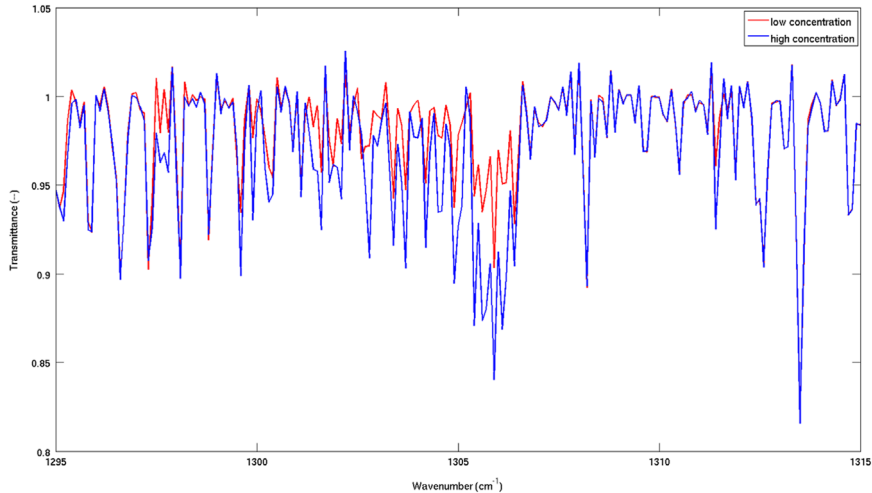


Fig. 13. Spectral window around the $\text{CH}_4 \nu_4$ band of the FTS simulated spectra corresponding to an altitude of 21.1 km in the occultation mode. The red spectrum corresponds to the CH_4 low concentration case and the blue one to the CH_4 high concentration case. Features which are insensitive to the change of methane concentration are from other Martian species (H_2O , CO_2) or solar lines. (For interpretation of the references to color in this figure legend, the reader is referred to the web version of this article.)

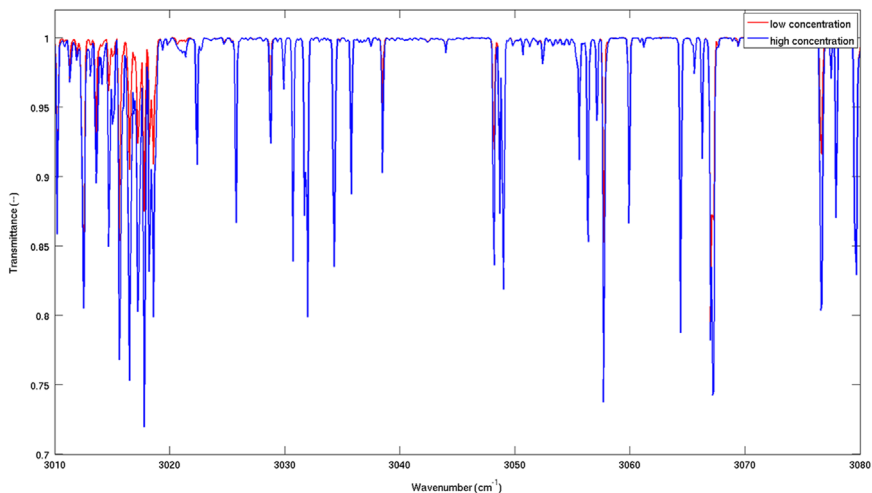


Fig. 14. Spectral window around the $\text{CH}_4 \nu_3$ band of the GA simulated spectra corresponding to an altitude of 21.1 km in the occultation mode. The red spectrum corresponds to the CH_4 low concentration case and the blue one to the CH_4 high concentration case. (For interpretation of the references to color in this figure legend, the reader is referred to the web version of this article.)

this was one important parameter differentiating the instruments. None of these changes had a fundamental influence on the fluctuations, i.e. they were always more or less present.

Among the 10 Monte Carlo realizations of simulated retrievals, we only plot in Figs. 15, 16, 18 and 19 a subset of 5 of them to show the weak influence of the first guess profile. The corresponding figures also exemplify, for individually retrieved profiles, their

consistency with the hypotheses of the OEM inversion including the *a priori* constraint specified by the \mathbf{S}_a matrix and the observational error defined by the \mathbf{S}_y matrix. In the following we provide explanations for the specific case of CH_4 retrievals in the 4 inversion configurations GA, FTS, L1/L1 and L2/L1.

To give some insights into these questions we can see that from Fig. 15, in the case of CH_4 that:

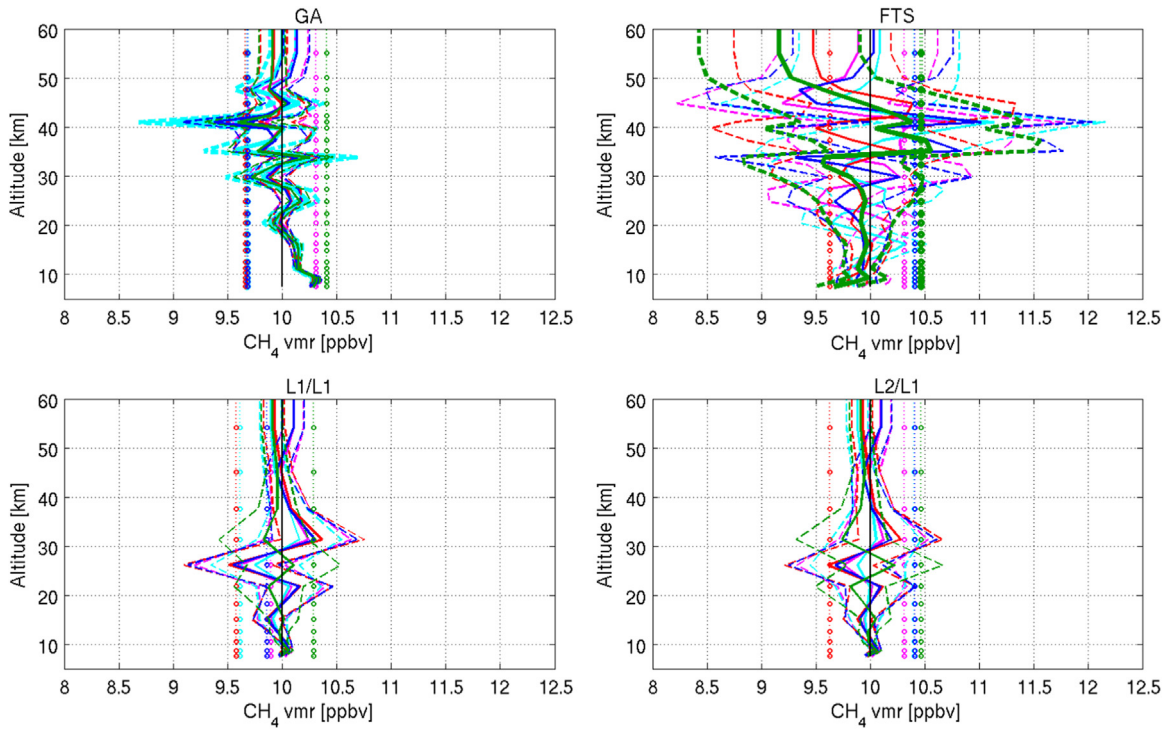


Fig. 15. 5 vertical profiles, out of the 10 realizations, in the case $L_s=30\text{--}60^\circ$ in low VMR conditions and in solar occultation. Upper left panel: GA instrument alone – Upper right panel: FTS instrument alone – Lower left panel: L1/L1 synergy – Lower right panel: L2/L1 synergy. The expected true solution is a constant 10 ppbv volume mixing ratio, in black. One single color represents one retrieval. The solid line shows the retrieved profile, the dashed line with markers represents the first guess and the uncertainty is given in dotted line. Note the largely expanded horizontal scale.

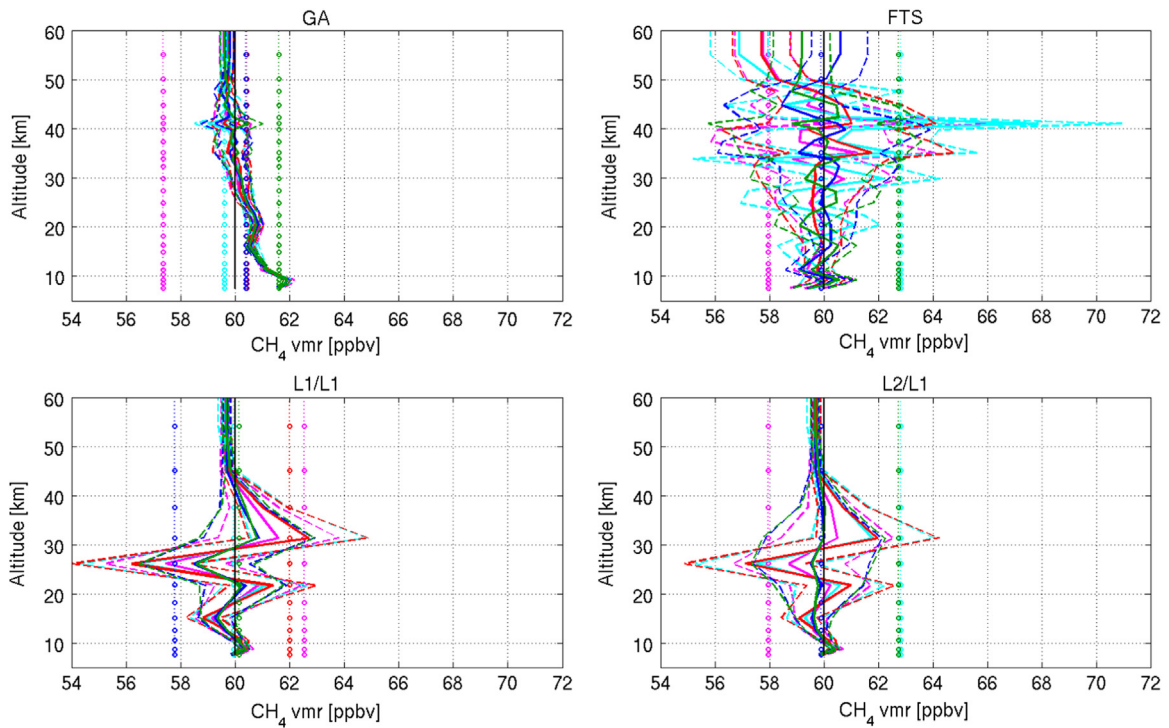


Fig. 16. 5 vertical profiles, out of the 10 realizations, in the case $L_s=30\text{--}60^\circ$ in high VMR conditions and in solar occultation. Upper left panel: GA instrument alone – Upper right panel: FTS instrument alone – Lower left panel: L1/L1 synergy – Lower right panel: L2/L1 synergy. The expected true solution is a constant 60 ppbv volume mixing ratio, in black. One single color represents one retrieval. The solid line shows the retrieved profile, the dashed line with markers represents the first guess and the uncertainty is given in dotted line. Note the largely expanded horizontal scale.

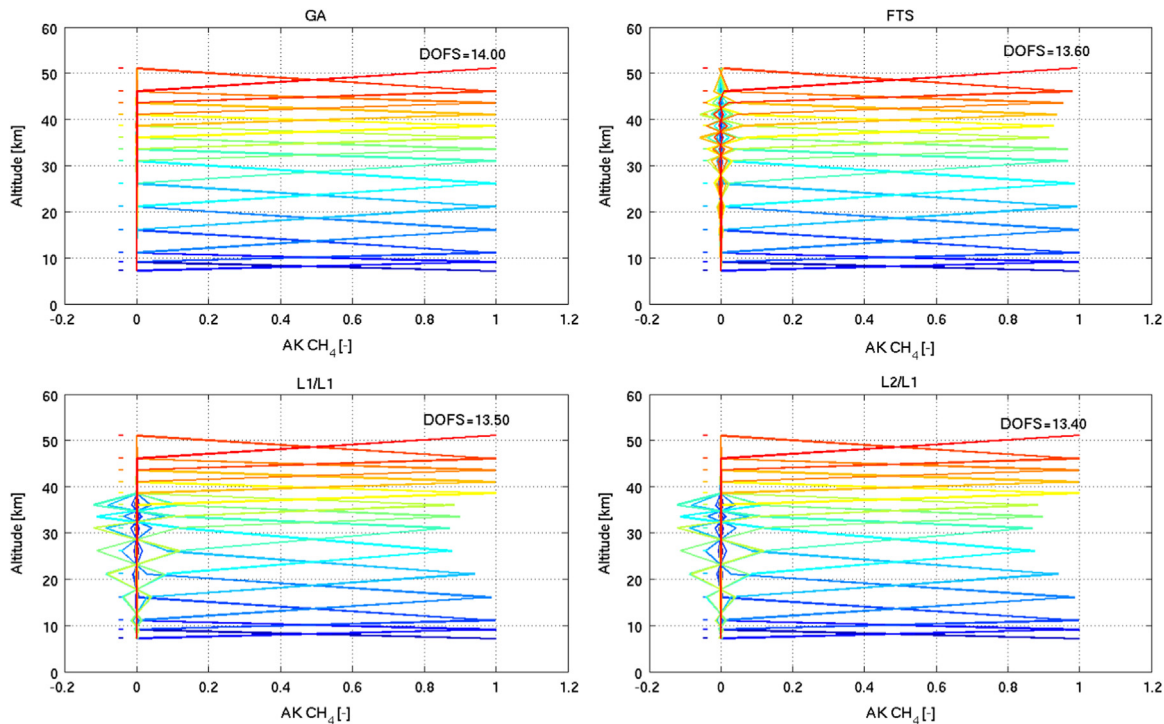


Fig. 17. Averaging kernels (AK) and degree of freedom for signal (DOFS) for CH_4 in the case $L_s=30\text{--}60^\circ$ in high VMR conditions and in solar occultation.

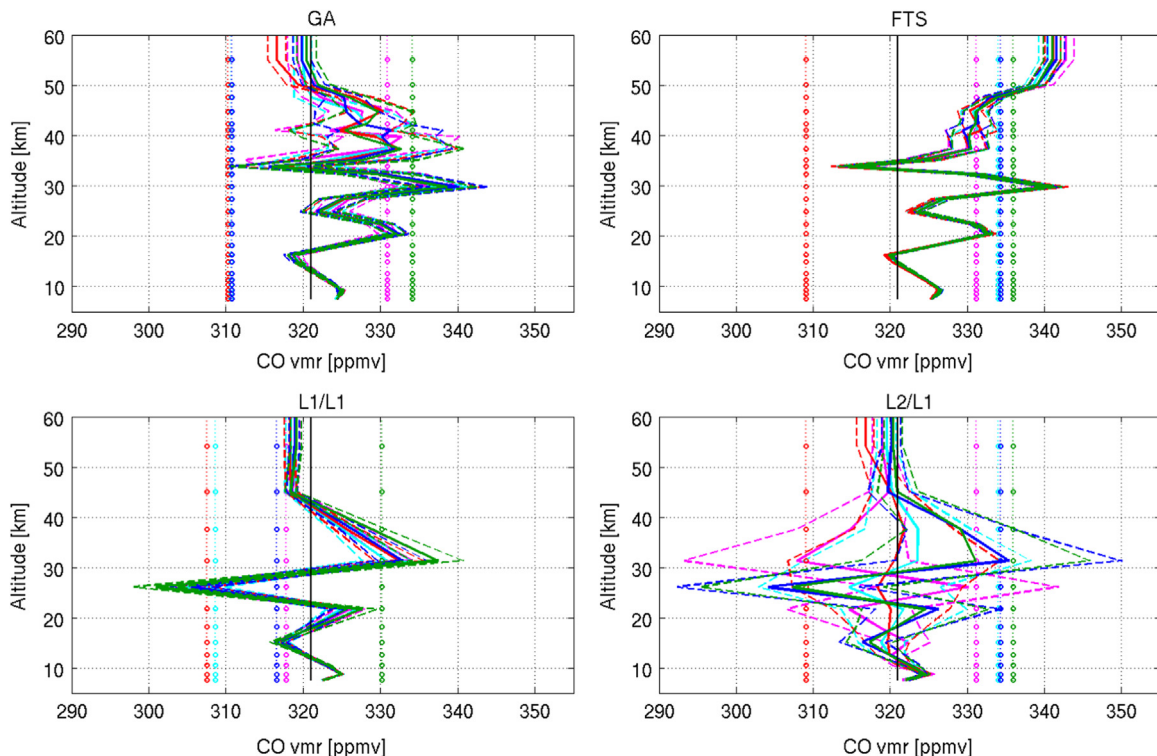


Fig. 18. 5 vertical profiles, out of the 10 realizations, in the case $L_s=30\text{--}60^\circ$ in low VMR conditions and in solar occultation. Upper left panel: GA instrument alone – Upper right panel: FTS instrument alone – Lower left panel: L1/L1 synergy – Lower right panel: L2/L1 synergy. The expected true solution is a constant 321 ppmv volume mixing ratio, in black. One single color represents one retrieval. The solid line shows the retrieved profile, the dashed line with markers represents the first guess and the uncertainty is given in dotted line. Note the largely expanded horizontal scale.

1. In the upper left panel (GA, strong ν_3 band of CH_4 around 3015 cm^{-1}), one of the retrieved profile (cyan thick) is reaching the truth (10 ppbv) even if the first guess is at 9.68 ppbv (in the range $\pm 5\%$ from the truth). The retrieved value at 41 km is 8.99

ppbv i.e. – 1.01 ppbv from the truth within 1σ i.e. the 10% uncertainty (diagonal term of \mathbf{S}_a) on a true value of 10 ppbv. The *a posteriori* 1σ error (derived from the error covariance matrix) of 0.13 ppbv is driven by the SNR (4000 for GA) and is consistent

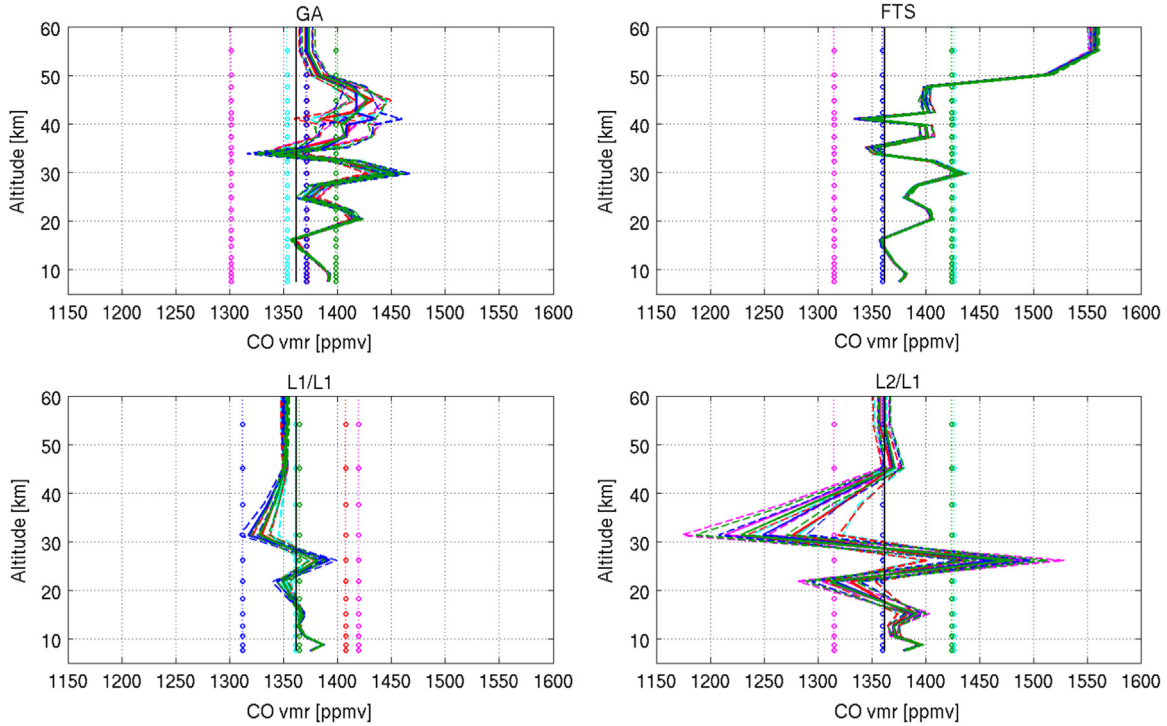


Fig. 19. 5 vertical profiles, out of the 10 realizations, in the case $L_s = 30\text{--}60^\circ$ in high VMR conditions and in solar occultation. Upper left panel: GA instrument alone – Upper right panel: FTS instrument alone – Lower left panel: L1/L1 synergy – Lower right panel: L2/L1 synergy. The expected true solution is a constant 1362 ppmv volume mixing ratio, in black. One single color represents one retrieval. The solid line shows the retrieved profile, the dashed line with markers represents the first guess and the uncertainty is given in dotted line. Note the largely expanded horizontal scale.

- with a difference of 0.01 ppbv between the mean value of the retrieved profile (10.01 ppbv) and the truth (10.00 ppbv).
2. In the upper right panel (FTS, weaker ν_4 band of CH_4 around 1306 cm^{-1}), one of the retrieved profile (green thick) is reaching the truth (10 ppbv) even if the first guess is at 10.46 ppbv (in the range $\pm 5\%$ from the truth). The retrieved value at 35 km is 10.56 ppbv i.e. +0.56 ppbv from the truth within 1σ i.e. the 10% uncertainty (diagonal term of S_a) on a true value of 10 ppbv. The *a posteriori* 1σ error (derived from the error covariance matrix) of 0.59 ppbv is driven by the SNR (1000 for FTS) and is consistent with a difference of 0.24 ppbv between the mean value of the retrieved profile (9.76 ppbv) and the truth (10.0 ppbv). The reduced precision in the FTS case is consistent with the reduced SNR compared to GA and the weaker intensity of the band used for the retrieval. The exact values of the respective SNR will only be known once the first spectra of both instruments are acquired in Martian orbit.
 3. In the lower left panel (L1/L1), the fluctuations of the FTS retrievals have been considerably reduced thanks to the simultaneous fit of both instruments. The peak-to-peak amplitude is consistent with the *a posteriori* 1σ error of the GA instrument which is the one constraining most the retrieval.
 4. In the lower right panel (L2 from FTS / L1 from GA), an additional reduction of the amplitude of the fluctuations is observed in relation to the fact that the column averaged VMR fixed by GA is better constraining the final retrieved profile.

The last spectrum being simulated at an altitude of +45 km above the surface (i.e. 51 km here), the values above that altitude will be forced to the value retrieved at the last level. This can be seen on the Figs. 15, 16, 18 and 19, from 51 km to the highest levels, the profile is constant.

The same type of arguments do apply for the CO retrievals in solar occultation mode shown in Figs. 18 and 19.

a) CH_4

For the FTS instrument, one spectral interval 200 cm^{-1} wide (from 1200 to 1400 cm^{-1}) was used to retrieve the VMR profile of CH_4 . This region corresponds to the ν_4 band, as shown on Fig. 13. Two smaller windows covering the ν_3 band were used to retrieve methane from the GA spectra, as shown on Fig. 14. In the case of synergies, the three methane windows were used for L1/L1 synergy and only the GA spectra were used to retrieve methane in the L2/L1 synergy. In this latter case, the FTS spectra were used to retrieve CO_2 and H_2O .

As a vertical profile is involved in this retrieval, the comparison between the different types of runs are not straightforward. One conclusion nonetheless, seems to be that L1/L1 synergy improves the determination of the profiles at low altitudes. This was expected since both spectral bands of CH_4 span a higher range of line intensity, the more intense lines being more adequate to sound higher layers (where the abundance of CH_4 is lower) and weaker bands playing a more important role in the lower layers. The gain of using L2/L1 synergy is not straightforward in this case.

Beside the comparison of the VMR profiles, we can also use the averaging kernels (AK) diagnostic. The AK represent the sensitivity of the retrieval to the true state. They are given in Fig. 17. The degree of freedom for signal (DOFS) is also indicated in the plots. It represents the theoretical number of pieces of information on the CH_4 profile available from the spectral measurements.

The values of the DOFS being lower in the case of synergies indicates that the level of information has not increased when using spectra from different instruments at the same time.

b) CO

To retrieve the vertical profile of CO, we used the 1-0 band measured by the FTS instrument and the 2-0 band measured by the GA instrument. In the L1/L1 synergy case, both bands are used.

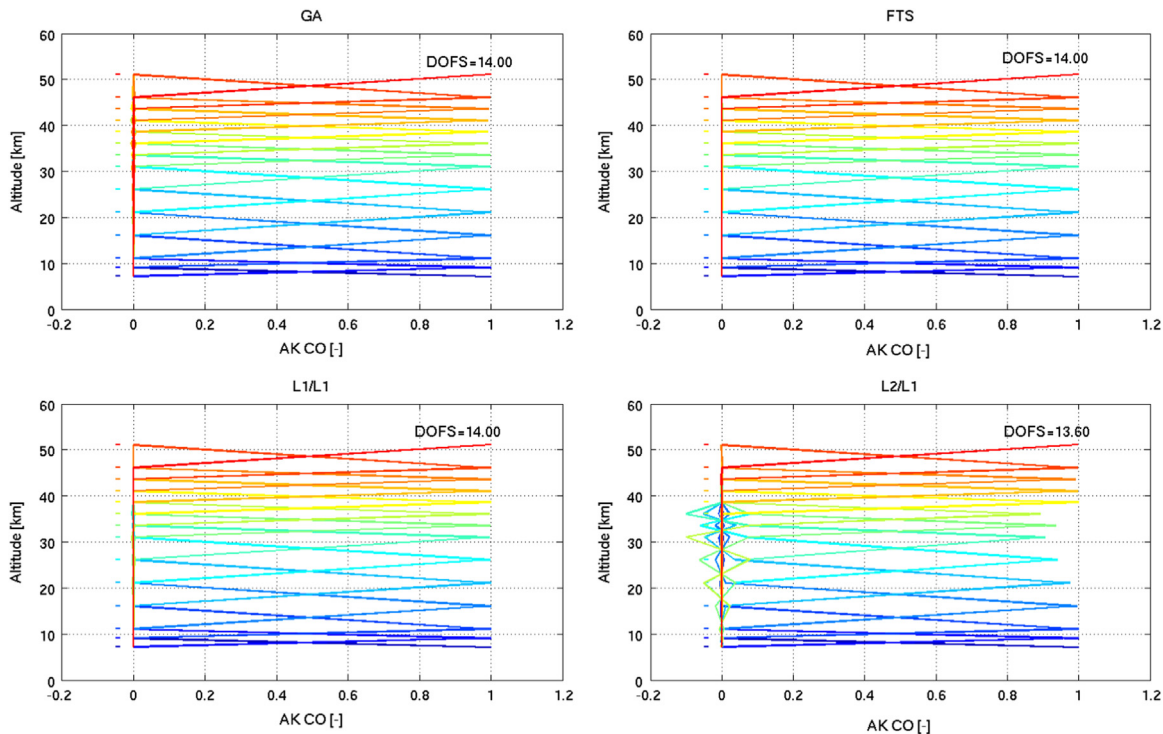


Fig. 20. Averaging kernels (AK) and degree of freedom for signal (DOFS) for CO in the case $L_s=30\text{--}60^\circ$ in high VMR conditions and in solar occultation.

In the L2/L1 synergy case, only the 2-0 band of GA spectra is used, as the FTS spectra are exploited to retrieve CO_2 and H_2O VMR profiles. The results of the 10 runs in the L_s period from 30 to 60° are given in Fig. 18 and Fig. 19 for low and high concentrations respectively. Similar conclusions as those derived for CH_4 can also be deduced for CO.

The comparison of the 4 retrievals indicates that the synergy L1/L1 is the retrieval method giving the results (colored line) closest to the true solution (green line).

Plotting the AK and calculating the DOFS is a useful tool to provide indication on the success probability of the retrievals. They are presented in Fig. 20. These results together with Figs. 18 and 19 demonstrate that the L1/L1 synergy is (as in nadir) the most successful one.

4. Conclusion

The goal of this theoretical study was to determine the impact of synergies between different instruments on board the same platform orbiting around Mars. This work has been undertaken with a particular focus on the ExoMars TGO 2016 mission, accommodating two IR instruments that might operate in a complementary way. A database of synthetic spectra was created taking into account the expected characteristics of two representative instruments, based on the known specifications of the EMTGO instruments available at the time of this study.

The systematic retrievals that have been performed show a positive impact of synergies in the quantification of CO while no noticeable improvement is expected in the detection/quantification of CH_4 . These results can be explained based on spectroscopic and instrument related arguments. The use of the ν_4 band of CH_4 is not very promising due to the low abundance of Martian methane and to the low spectral resolution and SNR of the FTS spectra considered in this study. For CO, however, both vibrational bands, i.e. the 1-0 around $4.7\ \mu\text{m}$ and the 2-0 around $2.3\ \mu\text{m}$ respectively measured by the FTS and GA instruments, provide interesting

synergistic possibilities.

Nevertheless these results must be considered with caution, as our study did not embrace all aspects of the Martian environment. Emissivity was considered as constant while it may vary spectrally [59]. Aerosols were not considered even though we know their importance in the Martian atmosphere. The retrievals themselves were also simplified as the vertical temperature profile was assumed to be known. Usually the atmospheric temperatures are obtained from the CO_2 density and therefore have an associated uncertainty. The assumption used in this study is excluding this additional uncertainty.

The instruments are in Martian orbit by now and more specific cases could be considered, especially taking into account the effect of aerosols or non-constant vertical profiles. More sophisticated inversions would lead to more time-consuming simulations and more complicated retrievals. However, without a better knowledge of the actual performances of the two instruments (particularly once the final orbit around Mars is reached) the expected results would most likely demonstrate the usefulness of synergistic retrievals from real NOMAD and ACS spectra (both spectrally and geometrically). The advantages presented here are theoretical and real data might lead to different results. The Monte Carlo approach chosen in this work was a way to convince us of the validity and robustness of our implementation of the optimal estimation method for a multi-instrument, multi-geometry and multi-spectral inversion of Martian spectra. Just a sensitivity analysis was insufficient to demonstrate the impact of the various possible synergies discussed in this paper. The exact SNR values will be refined once the orbit around Mars is stabilized. The knowledge of the shape (\mathbf{x}_a) and the *a priori* uncertainty (\mathbf{S}_a) of the methane profile will be refined by further observations or model calculations (as in [60]), but the results presented here are a good indication that our retrieval tools are mature enough and ready for an optimal scientific use of the NOMAD and ACS spectra soon to be acquired. This work aims to pave the way to more collaborative studies. Mars is orbited by a number of high-performance instruments and their scientific return might be improved through

synergistic retrievals. In order to assess the uncertainties related to emissivity, temperature profiles, aerosols loadings, etc., two studies are currently ongoing based on the Mars Express data focusing on H₂O and CO. Results of these will be published in the coming year.

Acknowledgements

This work was funded by the SIROCCO project under ESA contract number 4000107088 (with NOVELTIS as prime contractor). The study was proposed and supervised by A.G. Straume-Lindner and O. Witasse. The research was performed as part of the "Interuniversity Attraction Poles" program financed by the Belgian government (Planet TOPERS) and a BRAIN research grant BR/143/A2/SCOOP. The research leading to these results has received funding from the European Community's Seventh Framework Programme (FP7/2007–2013) under the Grant agreement no. 607177 CrossDrive and from the European Union's Horizon 2020 Programme (H2020-Compet-08–2014) under grant agreement UPWARDS-633127.

References

- [1] Rinsland CP, et al. Tropospheric Emission Spectrometer (TES) and Atmospheric Chemistry Experiment (ACE) measurements of tropospheric chemistry in tropical southeast Asia during a moderate El Nino in 2006. *J Quant Spectrosc Radiat Transf* 2008;109:1931–1942.
- [2] Antón M, et al. Validation of the MetOp-A total ozone data from GOME-2 and IASI using reference ground-based measurements at the Iberian Peninsula. *Remote Sens Environ* 2011;115:1380–1386.
- [3] Fraeman A, et al. Spectral absorptions on Phobos and Deimos in the visible/near infrared wavelengths and their compositional constraints. *Icarus* 2014;229:196–205.
- [4] Witasse O and Allen M. The ExoMars 2016 Trace Gas Orbiter. In: Proceedings of the 4th international workshop on the Mars atmosphere: Modelling and observations; 2011. Paris, France.
- [5] Neefs E, et al. NOMAD spectrometer on the ExoMars trace gas orbiter mission: part 1—design, manufacturing and testing of the infrared channels. *Appl Opt* 2015;54(28):8494–8520.
- [6] Vandaele AC, et al. Science objectives and performances of NOMAD, a spectrometer suite for the ExoMars TGO mission. *Planet Space Sci* 2015;119:233–249.
- [7] Koralev Ol, et al. ACS experiment for atmospheric studies on "ExoMars-2016" Orbiter. *Sol Syst Res* 2015;49(7):529–537.
- [8] Kaplan L, Connes J, Connes P. Carbon monoxide in the Martian atmosphere. *Astrophys J* 1969;157:187–192.
- [9] Clancy RT, Muhleman DO. Corrections regarding the Lellouch et al. (1989) analysis of Mars atmospheric ¹²CO and ¹³CO spectra. *Icarus* 1990;85(1):120–128.
- [10] Krasnopolsky V. Spectroscopic mapping of Mars CO mixing ratio: detection of north-south asymmetry. *J Geophys Res* 2003. <http://dx.doi.org/10.1029/2002JE001926>.
- [11] Encrenaz T, et al. Seasonal variations of the martian CO over Hellas as observed by OMEGA/Mars Express. *Astron Astrophys* 2006;459(1):265–270.
- [12] Krasnopolsky V, et al. Oxygen and carbon isotope ratios in the martian atmosphere. *Icarus* 2007;192(2):396–403.
- [13] Billebaud F, et al. Observations of CO in the atmosphere of Mars with PFS on board Mars Express. *Planet Space Sci* 2009;57(12):1446–1457.
- [14] Smith M, et al. Compact Reconnaissance Imaging Spectrometer observations of water vapor and carbon monoxide. *J Geophys Res* 2009;114:E00D03.
- [15] Sindoni G, Formisano V, Geminale A. Observations of water vapour and carbon monoxide in the Martian atmosphere with the SWC of PFS/MEX. *Planet Space Sci* 2011;59:149–162.
- [16] Krasnopolsky V. Variations of carbon monoxide in the martian lower atmosphere. *Icarus* 2015;253:149–155.
- [17] Formisano V, et al. Detection of methane in the atmosphere of Mars. *Science* 2004;306:1758–1761.
- [18] Geminale A, Formisano V, Giuranna M. Methane in martian atmosphere: average spatial, diurnal and seasonal behaviour. *Planet Space Sci* 2008;56(9):1194–1203.
- [19] Mumma MJ, et al. Strong release of methane on Mars in Northern Summer 2003. *Science* 2009;323(5917):1041–1045.
- [20] Villanueva GL, et al. A sensitive search for organics (CH₄, CH₃OH, H₂CO, C₂H₆, C₂H₂, C₂H₄), hydroperoxy (HO₂), nitrogen compounds (N₂O, NH₃, HCN) and chlorine species (HCl, CH₃Cl) on Mars using ground-based high-resolution infrared spectroscopy. *Icarus* 2013;223(1):11–27.
- [21] Webster C, et al. Mars methane detection and variability at Gale crater. *Science* 2015;347(6220):415–417.
- [22] Formisano V, et al. The Planetary Fourier Spectrometer (PFS) onboard the European Mars Express mission. *Planet Space Sci* 2005;53(10):963–974.
- [23] Murchie S, et al. Compact Reconnaissance Imaging Spectrometer for Mars (CRISM) on Mars Reconnaissance Orbiter (MRO). *J Geophys Res* 2007;112:E05S03.
- [24] Sprague AL, et al. Interannual similarity and variation in seasonal circulation of Mars' atmospheric Ar as seen by the Gamma Ray Spectrometer on Mars Odyssey. *J Geophys Res* 2012;117:E04005.
- [25] Sprague AL, et al. Mars' atmospheric argon: tracer for understanding Martian atmospheric circulation and dynamics. *J Geophys Res* 2007;112:E03S02.
- [26] Zurek RW, et al. Assessment of a 2016 Mission Concept: the Search for Trace Gases in the Atmosphere of Mars. *Planet Space Sci* 2011;59:284–291.
- [27] Vago J, et al. ExoMars Program: the next step in exploring Mars. *Sol Syst Res* 2015;49(7):518–528.
- [28] Vandaele AC, et al. Optical and radiometric models of the NOMAD instrument part I: the UVIS channel. *Opt Express* 2015;23(23):30028–30042.
- [29] Thomas IR, et al. Optical and radiometric models of the NOMAD instrument – Part II: the IR channels – SO and LNO. *Opt Express* 2016;24(4):3790–3805.
- [30] Trokhimovskiy A, et al. Middle-infrared echelle cross-dispersion spectrometer ACS-MIR for the ExoMars Trace Gas Orbiter. *SPIE Infrared Remote Sens Instrum XXIII* 2015:960808.
- [31] Trokhimovskiy A, et al. Near-infrared echelle-AOTF spectrometer ACS-NIR for the ExoMars Trace Gas Orbiter. *SPIE Infrared Remote Sens Instrum XXIII* 2015:960809.
- [32] Vandaele AC, et al. NOMAD, a spectrometer suite for Nadir and Solar Occultation observations on the ExoMars Trace Gas Orbiter. In: Proceedings of the 4th international workshop on the Mars atmosphere: Modelling and observations. Paris, France; 2011.
- [33] Patel MR, et al. NOMAD spectrometer on the ExoMars trace gas orbiter mission: part 2—design, manufacturing and testing of the UVIS channel. *Applied Optics*. in preparation; 2016.
- [34] Trokhimovsky A, et al. Atmospheric Chemistry Suite (ACS): a set of Infrared Spectrometers for Atmospheric Measurements on Board ExoMars Trace Gas Orbiter 15 mn. In: Proceedings of the Fifth international workshop on the Mars atmosphere: Modelling and observations. Oxford, UK, January 13–16 2014; 2014.
- [35] Liuzzi G, et al. Physical inversion of the full IASI spectra: assessment of atmospheric parameters retrievals, consistency of spectroscopy and forward modelling. *J Quant Spectrosc Radiat Transf* 2016;182:128–157.
- [36] Vandenbussche S, et al. Retrieval of desert dust aerosol vertical profiles from IASI measurements in the TIR atmospheric window. *Atmos Meas Tech* 2013;6:2577–2591.
- [37] Razavi A, et al. Characterization of methane retrievals from the IASI space-borne sounder. *Atmos Chem Phys* 2009;9:7889–7899.
- [38] August T, et al. IASI on Metop-A: operational Level 2 retrievals after five years in orbit. *J Quant Spectrosc Radiat Transf* 2012;113(11):1340–1371.
- [39] Rothman LS, et al. The HITRAN2012 molecular spectroscopic database. *J Quant Spectrosc Radiat Transf* 2013;130:4.
- [40] Sung K, Varanasi P. CO₂-broadened half-widths and CO₂-induced line shifts of ¹²C¹⁶O relevant to the atmospheric spectra of Venus and Mars. *J Quant Spectrosc Radiat Transf* 2005;91:319–322.
- [41] Gamache RR, et al. CO₂-broadening of water vapor lines. *J Mol Spectrosc* 1995;170(1):131–151.
- [42] Gamache RR, Laraya AL, Lamouroux J. Half-widths, their temperature dependence, and line shifts for the HDO-CO₂ collision system for applications to CO₂-rich planetary atmospheres. *Icarus* 2011;213(2):720–730.
- [43] Brown LR, Humphrey CM, Gamache RR. CO₂-broadened water in the pure rotation and ν₂fundamental regions. *J Mol Spectrosc* 2007;246(1):1–21.
- [44] Vandaele AC, et al. Composition of the Venus mesosphere measured by SOIR on board Venus Express. *J Geophys Res* 2008. <http://dx.doi.org/10.1029/2008JE003140>.
- [45] Sneep M, Ubachs W. Direct measurement of the Rayleigh scattering cross section in various gases. *J Quant Spectrosc Radiat Transf* 2005;92(3):293–310.
- [46] Hase F, et al. The ACE-FTS atlas of the infrared solar spectrum. *J Quant Spectrosc Radiat Transf* 2010;111(4):521–528.
- [47] Fonti S, Marzo GA. Mapping the methane on Mars. *Astron Astrophys* 2010;512:A51.
- [48] Allen MA, et al. Is Mars Alive? *EOS Trans Am Geophys Union* 2006;87:433–439.
- [49] Daerden F, et al. A solar escalator on Mars: self-lifting of dust layers by radiative heating. *Geophys Res Lett* 2015;42(18):7319–7326.
- [50] Geminale A, Formisano V, Sindoni G. Mapping methane in Martian atmosphere with PFS-MEX data. *Planet Space Sci* 2011;59:137–148.
- [51] Webster Christopher R, et al. Mars methane detection and variability at Gale crater. *Science* 2014.
- [52] Vandaele AC, Kruglanski M, and De Maizière M. Modeling and retrieval of Atmospheric spectra using ASIMUTin In: Proceedings of the First 'Atmospheric Science Conference'. ESRIN, Frascati, Italy; 2006.
- [53] Drummond R, et al. Studying methane and other trace species in the Mars atmosphere using a SOIR instrument. *Planet Space Sci* 2011;59:292–298.
- [54] Rodgers CD. Inverse methods for atmospheric sounding: theory and practice. In: Hackensack NJ, editor. World Scientific. University of Oxford.
- [55] Nevejans D, et al. Compact high-resolution space-borne echelle grating spectrometer with AOTF based on order sorting for the infrared domain from

- 2.2 to 4.3 μm . *Appl Opt* 2006;45(21):5191–5206.
- [56] Robert S, et al. Expected performances of the NOMAD/ExoMars instrument. *Planet Space Sci* 2016;124:94–104.
- [57] Boynard A, et al. Seven years of IASI ozone retrievals from FORLI: validation with independent total column and vertical profile measurements. *Atmos Meas Tech Discuss* 2016;9:4327–4353.
- [58] Tikhonov A-N. On the solution of incorrectly stated problems and a method of regularization. *Dokl Acad Nauk SSSR* 1963;151:501–504.
- [59] Fraeman AA, et al. Analysis of disk-resolved OMEGA and CRISM spectral observations of Phobos and Deimos. *J Geophys Res* 2012;117:E00J15.
- [60] Viscardy S, Daerden F, Neary L. Formation of layers of methane in the atmosphere of Mars after surface release. *Geophys Res Lett* 2016;43:1868–1875.